Master's Thesis

Design of Lidar-system

Martin Andersson
Johan Kjörnsberg

Department of Electrical and Information Technology,
Faculty of Engineering, LTH, Lund University, June 2014.

Design of Lidar-system

Martin Andersson
mola.tf@gmail.com
Johan Kjörnsberg
johan.kjornsberg@gmail.com

Department of Electrical and Information Technology
Lund University

Advisors:
Anders Nejdel
Carl-Axel Alm

June 26, 2014

Printed in Sweden
E-huset, Lund, 2014

Abstract

This thesis is intended to be a first investigation into the design of a laser range finding system with sufficient performance to be able to be implemented in a LIDAR system. All parts of the system including the transmitting and receiving circuitry as well as the optical setup is to be considered. An aim of this project is to use ordinary off-the-shelf components.

A literature study on different laser range finding architectures and existing products has been performed, as well as a theoretical analysis of different photodetectors. Eye safety aspects when using lasers have been reviewed, and proper precautions were taken. The chosen circuit topology has been simulated to ensure correct operation and to fine tune component values.

A first PCB layout was created and realised, and a second revision was done to improve discovered shortcomings of the first revision. The performance of the two systems has been evaluated experimentally, especially the second revision.

Performance wise, the designed system has been shown to measure distances of up to 27 m with a standard deviation of 15 cm at an estimated measurement speed of at least 8 kHz.

Acknowledgements

We would like to thank our supervisors Anders Nejdel (EIT) and Carl-Axel Alm for inspiration and guidance throughout the project. We would also like to thank those who kindly answered our numerous questions and lent us equipment, especially our closest colleagues and Andreas Gustafsson for valuable input in all parts of the process.

Table of Contents

List of Figures

List of Tables

Chapter 1

Introduction

The central theme of this Master's Thesis is range finding. There are numerous ways of measuring distance and each way has its advantages, whether it be accuracy, speed or practical considerations. It stands to reason that the application dictates which technology should be used for measuring. For instance, one might be inclined to use e.g. a ruler for measuring the distance between two points on a piece of paper. This method is however inconvenient for measuring the distance between the earth and the moon, where other methods are more suitable.

The distances which are considered in this thesis are short to medium range, i.e. from about one meter up to tens of meters. Measurement accuracy is not critical, but an error within a few centimeters is desirable considering the magnitude of the distances to be measured.

The main focus will be on Laser-based measurement technologies. The idea of using lasers for range finders is not a new one as it has been discussed several decades ago in e.g. [1]. There are several commercial products available in many different performance and price ranges, as will be discussed in section 1.2 below. An advantage of using laser over other non-contact technologies such as ultrasound or microwaves for range finding is that the smaller wavelength of light allows it to be focused into a smaller spot, which increases spatial resolution in the plane. Furthermore, narrow optical bandpass filters provide a convenient way to filter out light of wavelengths other than the laser wavelength used, i.e. noise, which potentially increases the signal to noise ratio (SNR). [3]

LIDAR (Light Radar) refers to a device where the distance to objects in the plane of the device is measured with some specified update rate. As the name suggests the device uses light, typically a laser beam, for measuring. The output of the device can be represented as a two-dimensional map with the device in the center and dots representing the distance to the objects surrounding it, i.e. a typical radar image as shown in figure 1.1.

Figure 1.1: A typical 2D radar image which may be the output of a LIDAR system. The detector is placed in the center and the sweeping beam represents the laser beam. The lighter dots are targets, and the distance from them to the center of the image represents their distance from the detector. [2]

1.1 Motivation

The aim of this thesis project is to design a laser range finder which could be integrated in a LIDAR system. The upper limit of distance considered for measuring is 50 m under varying target reflectivities. Measurement accuracy is to be kept ideally within a few centimeters. A study of existing laser range finding architectures is to be performed, and a candidate for implementation is to be chosen. After implementation the performance of the prototype shall be evaluated with respect to upper distance limit, measurement speed and accuracy under different target reflectivities.

There is a number of laser range finders commercially available, but it seems to the authors that they are typically divided into two categories. One of them is the high priced[1] ones that both have high performance, in terms of range (SAAB Heimdall) [4], accuracy (DLS-CH15) [5] and speed (Hokuyo UTM) [6]. Devices that possess a linear combination of these properties (Leica C10) [7] also exist. The other is the cheap ones, which may either be slow (Prexiso and Parallax) [8] [9] or both (Parallax) [9]. The options between these categories, i.e. range finders that have decent range and accuracy capabilities while still being moderately fast seem to be limited. The actual performance of these detectors will be discussed in section 1.2 below.

With few exceptions, ("Homebrew LRF") [10] and some forum threads [11] [12], there does not seem to be many advanced "homebrew" devices realized or plans to do so yet to fill this gap, as most of these projects aim for simpler, albeit

[1]It is usually difficult to find pricing information on truly high end products without requesting a price quote, and even then one is not sure of getting an answer. However, by comparing to what is commercially available one may extrapolate, but in this thesis the authors are content simply stating that the device is expensive, or possibly very expensive.

cheap, devices. [13] Granted, what is considered a high price depends on the situation, but to introduce some type of scale around 100 USD is considered the lower bound of expensive in this project.

Following discussions on various electronics hobbyist forums, there seems to be a demand for such medium cost but moderately fast laser range finders for implementing in certain robot projects, typically for obstacle avoidance purposes. [12] Salvaging the range finder in existing products, e.g [14], fails to yield sufficient performance or is practically difficult, and the expensive range finders are not an option. As mentioned there are few proper guides for building one yourself. An aim of this project is to realise such a device or system with "ordinary" components, i.e. ones that are available off the shelf with large component distributors and are not too expensive. If such a device is realised, then the authors imagine that there would be no shortage of interesting applications. For practical reasons such as alignment and focusing, and as an eye safety precaution, a visible laser beam emitted from a suitable laser diode will be used in this project.

Designing a laser range finder is an interdisciplinary task. It involves electronics for the transmitting and receiving circuits and signal processing, as well as optics for the laser and also some biology where laser eye safety is concerned. Part of this project as an initial study on the subject is to map out what parameters matter the most and what parts of the system is most critical for performance.

1.2 Existing products

As mentioned above there exist many commercial laser range finders. This section is intended to provide an overview of what is available in terms of performance and price. A short description of the theory of operation for each device, along with speculation where details are scarce, is given. The details are covered in section 2.

Beginning at the expensive end there is the Leica Gesosystems C10 ScanStation system. [7] This device is used to map its surroundings with millimeter precision. This is done by sweeping a laser beam over the surroundings and measuring the distance to millions of points with a speed of 50 000 points/s. An integrated camera is used for color mapping, and all this information is fed into a computer which by using CAD software creates a highly accurate computer model of the space in question. The datasheet states that it uses a pulsed laser, so one might expect that it uses the time of flight measurement principle. There is also the Leica HDS6200 [15] which operates by instead measuring the phase difference between transmitted and received light. This device can measure the distance to up to a million points per second. Sadly, no pricing information was found for the HDS6200, but the latest pricing information for the C10 model was that it retails at USD $102375.00 [7].

Continuing on the expensive end, there is the Heimdall laser range finder from SAAB [4] which has a maximum range of 20 km. In the product overview it is stated that the pulse repetition rate is 1 Hz, which suggests that it is based on the time of flight method. No pricing was found, but given its performance and the fact that it uses a diode-pump solid-state laser instead of a simple laser diode as source, it is expected to be very expensive.

A little less expensive is the Hokuyo UTM-30LX [6], which retails at USD $4,974. The range is limited to 30 m, but it sweeps the beam over 270 degrees every 25 ms, with measurement points separated at 0.25 degrees. The datasheet makes no mention of what type of technology is used, but the laser source is at least eye safe under all circumstances.

Entering now the lower price range there is the SICK DT50Hi [16] which is in the USD $1,000 class. It uses a pulsed eye safe laser which implies that the technology is time of flight. It claims to have a response time of down to 15 ms, and accuracy of 7 mm.

At USD $99 one can buy the RB-Plx-257 range finder [9], which uses the parallax method. It employs a CMOS camera which captures an image of the area illuminated by the laser dot, and using the coordinates of the laser dot in this image, the distance is calculated using simple trigonemtric formulas. The device is slow with a sample rate of 1 Hz, and its distance is limited to 2.4 m.

There is a variety of handheld laser range finders available, and an example is the PCE-LDM 50 [17] for about USD $80. This has a range of 50 m and gives a measurement result "within seconds" of pressing the button.

At the lower end of the price range, there is for instance the laser range finder incorporated in the Vaccuum Cleaner from Neato Robotics [14]. It is used for 360 degrees mapping of the room to be cleaned, which enables object avoidance and planning in advance the cleaning route. The range finding unit itself, if it was built at home, could potentially cost as little as USD $30 to realize. [18] The technique used is again the parallax method, but in this implementation an invisible laser is used.

Chapter 2

Laser range finder architectures

As indicated by the variety of commercial laser range finders available, there are several architectures which could be used when designing a LIDAR system. This chapter is intended to provide an overview of the architectures which are relevant for this project, as well as to discuss advantages and drawbacks of each of them. Finally, a topology is chosen for implementation.

A first consideration, which applies to all receiver architectures discussed in this chapter, concerns the emitted and received optical power of the Laser. Since eye-safe operation of the Laser is preferred, the optical output power is limited which limits the the received power at the photodetector. Ultimately this limits the maximum distance that can be measured, due to the signal level falling below the noise floor.

2.1 Quadrature phase detection

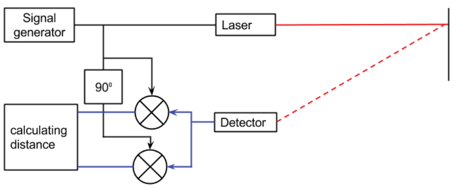

Figure 2.1: Illustration of a quadrature distance meter.

In this scheme a signal generator is used to generate a signal v_1 with a certain waveform and frequency f_m. The laser diode driver circuit then uses this signal to modulate the amplitude of the emitted laser beam. The emitted laser light is reflected by an object at a certain distance d from the setup, and is measured by a photo diode serving as detector. See figure 2.1 This gives rise to a signal v_2 with frequency f_m, the same as v_1, but there will be a phase difference θ between them due to that v_2 has travelled a total distance of $2d$ longer than v_1.

The phase difference will be measured using mixers. A mixer is a device whose input is two periodic signals, with frequencies f_1 and f_2, and whose output are signals with the difference and sum frequencies as well as harmonics. This is achieved through multiplying the input signals in the time domain, and to be able to do this the device must be nonlinear. Any nonlinear device can be used as a mixer, for instance a diode. To illustrate the operation of a mixer, two sine shaped waves $v_1 = A \cdot \sin(2\pi f_1 \cdot t)$ and $v_2 = B \cdot \sin(2\pi f_2 \cdot t)$ are considered. Multiplying them and using trigonometric identities gives the results in equation 2.1.

$$v_1 \cdot v_2 = \frac{AB}{2}[\cos(2\pi(f_1 - f_2)t) - \cos(2\pi(f_1 + f_2)t)] \tag{2.1}$$

Putting v_2 as the reflected signal, it is split and one instance is mixed with v_1 producing the result I and the other is mixed with v_1', which is v_1 phase shifted by 90°, producing the result Q. This results in a vector in the I-Q -plane, see figure 2.2, whose argument is the phase difference θ between v_1 and v_2 and its magnitude gives the amount of light reflected from the object that actually reached the detector. Since the frequency of both signals is f_m, the time t it took for the laser light to travel a distance of $2d$ is easily calculated from the phase difference θ. Using then the speed of light c, the distance to the object d is calculated, see equation 2.2.

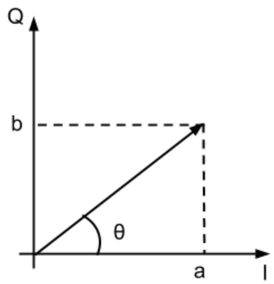

Figure 2.2: I-Q -plane illustration.

$$d = \frac{\theta c}{4f\pi} = \frac{arctan(b/a)c}{4f\pi}; \tag{2.2}$$

The benefits of using quadrature phase detection are that both the phase difference θ and information about the reflectance of the object measured on are obtained. This may be of interest in future applications, for instance if the reflectance of the objects measured on often varies. The reflectivity information may then be used to complement the distance measurement, providing an additional dimension and degree of freedom to the system. This may be taken advantage of in the form of determining the presence of some specific objects, or even classification of objects present, rather than just measuring the distance to them. Furthermore, the distance calculations are performed rapidly by a circuit, and since they are based on the phase information of continuous waves, high measurement rates, depending on f_m, are expected to be possible. Finally, the circuitry is not very complicated, and since the values of f_m investigated in this project will range between 0.1 MHz and 100 MHz, widely available conventional components in both the driver and receiving circuit can be used without high frequency effects becoming dominating.

A limitation of this technique is that at a fixed frequency f_m, when the distance to the object increases the phase shift between the transmitted and reflected signal increases as well. A phase shift of 360° is for the receiver equivalent to a phase shift of 0°, which means that the distance measured will vary periodically depending on the modulation frequency. Thus, a scheme which removes these possible ambiguities is needed, and such ideas will be discussed in more detail in section 11.4.1. To mention it now though, such a scheme will most likely use a combination of different modulation frequencies. A lower frequency allows a larger distance to be measured without ambiguities than a higher frequency. Thus, combining two such frequencies that are not harmonics of each other, the lower of them would be used to decide the order of the ambiguity interval for the higher frequency.

There is another discussion implied in the general scheme described above, namely the accuracy of the distance measurement. This accuracy is directly given by the accuracy by which the phase difference is measured. Assuming that the phase difference accuracy is independent of frequency, it follows that for a given distance d two modulation frequencies $f_1 < f_2$ yield different distance accuracy. For instance, if $f_1 = 0.1$ MHz and $f_2 = 10$ MHz and the receiver can measure phase difference accurately to $e = 1°$, then the distance accuracy becomes as in equation 2.3.

$$d_{acc} = \frac{1}{f} \cdot \frac{e}{360} \cdot c \tag{2.3}$$

which gives $d_{acc} = 8.33$ m for f_1 and $d_{acc} = 8.33$ cm for f_2. A technique using multiple modulation frequencies may thus offer both long range and good accuracy. See figure 2.3 for a system using two different modulation frequencies.

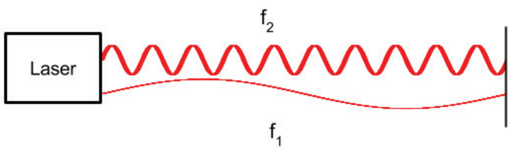

Figure 2.3: Illustration of a system using two different modulation frequencies. Here f_1 provides a crude distance approximation while f_2 provides accuracy.

2.2 Time of Flight-measurement of laser pulses using TDC

The idea is to emit short pulses of laser light and then measure the time for them to return. The distance to the object is then the measured time multiplied with half of the speed of light. The time is measured with a TDC, time to digital converter, which could measure the time with a sensitivity of 90 ps , which gives a resolution in distance of 13.5 mm but could be reduced with averaging over several pulses.

The time of flight method has the advantage that it is a technique which is very easy to understand and thereby to implement. Increasing the maximum transmited power is also easy as discussed in section 11.4.1 A drawback is limited measuring rate since one pulse at a time is sent. However, quite high rates are still possible since the speed of light is so high. Using certain types of averaging, measurement rates of up to 500 kHz are possible.[20] . Furthermore, the TDC could cause a problem since its power consumption at high measuring rates may be as high as 20 W [19] which in some cases may cause problems with cooling.

2.3 Chirped laser pulses

This method is based on laser pulses which have been amplitude modulated linearly from a frequency f_1 to a frequency f_2 over the time domain pulse length. Upon receiving the reflected pulse after a time Δt, the locally generated signal is mixed with the received signal. A Fast Fourier Transform is then used to obtain the beat frequency, which is directly related to the distance to the object. The advantage of using this method is that less emitted pulse power is needed to obtain the necessary information. A drawback with this approach is that the system is more complex than the quadrature receiver system. For instance while the FPGA in the camera used can perform the FFT operation at little extra cost, it still has to be programmed correctly, hence the added complexity. [22]

2.4 Coherent detection

Coherent detection is a system where the mixing operations are done in the optical domain.[21] This could be used both in a phase detection system and when chirped laser pulses are used. This method has the advantage of better Signal-to-Noise ratio than the previous architectures since it is dominated by shot noise rather than thermal noise in the circuit components.[22]

The main disadvantages are that more advanced optical components are needed, which implies higher cost, as well as the knowledge of how to use them, which the authors do not possess. Furthermore, problems may arise when multiplexing two optical signals, and due to there being a phase difference between the two signals, random errors will be produced in the mixing.

2.5 Choosing technology

An ambition in this project is to maximize measurement speed and so a phase detection system is favoured over TOF and chirped pulses. Coherent mixing is rejected since the design would be too complex for consideration in this project.

Thus, initial efforts were focused on designing a range finder based on quadrature phase detection as the receiver circuit. A complete system overview as it was implemented is presented in figure 2.4. This schematic will be shown in the beginning of certain chapters, with the blocks corresponding to the topic of that chapter highlighted.

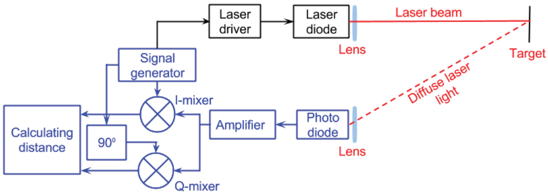

Figure 2.4: A schematic illustration of the complete system as it was implemented.

Chapter 3

Optics

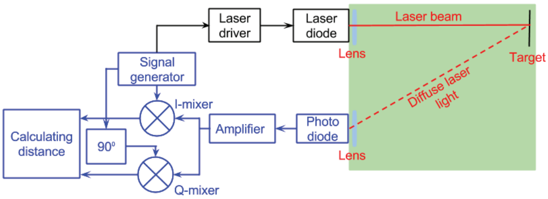

In this chapter optical considerations will be discussed.

The discussion of optics in this chapter will range from Laser physics to the lenses required for the transmitting and receiving circuits. An analysis of the amount of light diffusely reflected from a target is done, as well as a discussion of detector size and optimal placement relative the transmitter.

3.1 Return light analysis

The main objective of the receiver optics is to collect as much light to the photodetector as possible. This could be done with either mirrors or lenses. The advantage that mirrors usually provide is that there is no chromatic abberation which could be a problem for lenses. In this study this is not a problem however since monochromatic light will be used. Mirrors have the disadvantage of being difficult to mount in the test environment, and therefore lenses is used in this study.

Plano-convex lenses are used since a more advanced optical system is not expected to be required. The size of the lens sets the amount of light focused on the photodetector. The three different diameter lenses that will be investigated are 25 mm, 50 mm and 75 mm.

To estimate the received power, P_r, for a certain transmitted power, P_t, it is assumed that no power is lost on the way to the target which is at an distance d. The atmospheric attenuation of visible light is neglectably small for the distances considered, and so this approximation is valid.[27] The target have a reflectivity R and reflects in all directions, i.e. diffusely. The received power in a detector with area A_d could then be approximated with equation 3.1. The minimum received power is calculated for different lenses in a worst case scenario in the problem description, maximum distance 50 m and minimum reflectivity of 6 %. If 1 mW is transmitted minimum received power is given in table 3.1 for different sizes of lenses.

$$P_r = P_s \cdot R \cdot \frac{A_d}{4\pi d^2} \tag{3.1}$$

A_l [mm]	P_r [pW]
25	0.93
50	3.75
75	4.22

Table 3.1: Received optical power for different lenses.

Additional optics for the receiver includes an optical bandpass filter to reduce noise from ambient light. Here it has to be considered that all additional optics introduce transmission loss. For this reason measuring both with and without a bandpass filter is investigated.

3.2 Free space laser optics

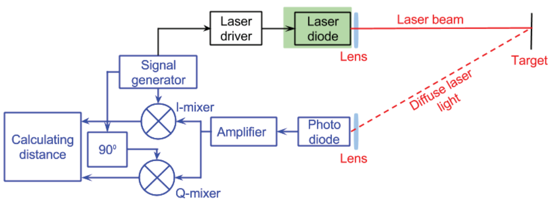

In this section the laser source is examined.

In this project the aim is to employ a laser for range finding with some specified accuracy. Depending on the actual demands on system performance and on the situation, the properties of the laser used may be limiting. These include wavelength stability and noise. There is a variety of different laser sources, e.g. gas source lasers or solid state pumped lasers. These systems are generally good with respect to these parameters, but they are rather complex systems.

Along the aim of the thesis to use only ordinary components, essentially the only choice is the semiconductor laser diode. Furthermore, an advantage of using this type of device is that its output power may be modulated simply and directly by the bias current.

A laser diode is a semiconductor device which emits coherent light of a single wavelength. It is essentially a pn-junction which is forward biased. Electrons and holes recombine in the depletion region, causing emission of photons with a certain energy. This energy depends on the bandgap of the semiconductor used, and may thus be tailored for a specific need.

The usual type of laser diode consists of a Fabry-Perot cavity. In a semiconductor material, these cavities usually have lengths around 300 μ m [31], and due to this small length, the output light is highly divergent and needs to be collimated to produce a well defined beam. Depending on the application one may use special collimators, but in this project a plano-convex lense suffices. It is placed in such a way that it focuses the LD light at infinity by placing the LD in the focal point as shown in figure 3.1. This lens may also have some coating optimized for a certain wavelength.

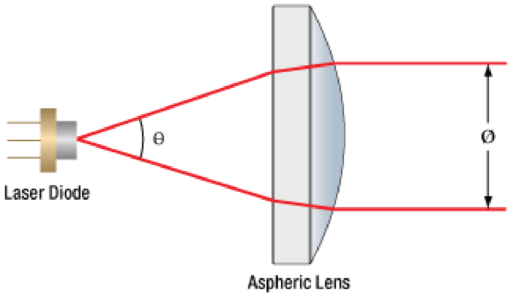

Figure 3.1: Illustration of the collimation of a Laser diode beam. Here Θ represents the divergence angle of the laser beam, and $\varnothing$ is the beam diameter after collimation. [23]

Furthermore, an assortment of neutral density (ND) filters with different transmission properties might be needed. ND-filters attenuate visible light equally over the entire spectrum and are typically specified with a certain transmission coefficient. Their use in this project is two-fold. The first use is related to eye-safety. Depending on the rated optical output power of the chosen LD, it may be advantageous to modulate the laser beam at intensities which are not eye-safe and then use ND-filters to attenuate the light to eye-safe levels.

The second use is for convenience when performing measurements with the device. Placing ND-filters in the path of the light will serve as attenuators to simulate the received optical power at different distances measured without actually moving or redirecting any equipment.

3.2.1 Detector size and placement

The experiment setup is shown in figure 3.2. For optimum performance at long distance the detector should be placed in the focal point, f, of the lens. Long distance is the most important consideration since it returns the least amount of light as discussed in the previous section. At shorter distances this makes the laser spot out of focus on the detector. To estimate how spread out the laser point is at the focal length for an object at a specific length, $S1$, first the focus point , $S2$, have to be calculated. This is done using the thin lens equation 3.2. The vertical position is then calculated using equation 3.3. Finally, the distribution, s, is calculated with simple trigonometry.

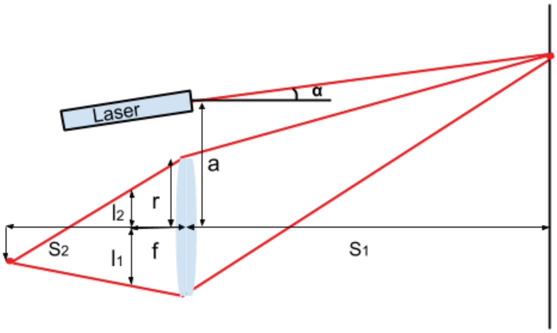

Figure 3.2: Schematic of optics.

$$\frac{1}{S_1} + \frac{1}{S_2} = \frac{1}{f} \tag{3.2}$$

$$M = -\frac{S_2}{S_1} \tag{3.3}$$

To investigate the different parameters a Matlab script is used to produce a graph where the position of s is plotted as a function of S_1. First the distance of the laser from the detector is varied when a $r = 7$ mm lens is used and since the transmitting laser has to be outside of the lens, a distance 40 mm from the detector is the minimum distance tested. The result is shown in figure 3.3 and here it is clear that the laser should be placed as close to the detector as possible. Otherwise refocus for different distances is needed.

The impact of the angle of the laser in respect to the lens optical axis is examined by testing different angles, see figure 3.4. The angular is of less importance since it mainly changes where the point is focused, the position does not change much for different distances for larger angles. The objective is to keep the angle at zero, but it is not as critical as keeping the laser close to the detector.

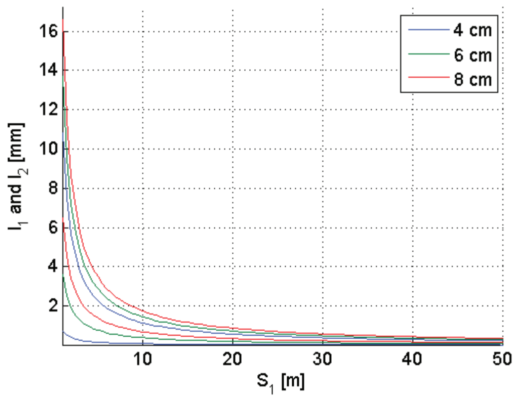

Figure 3.3: Simulations for testing laser spot in focal point when a is varied. r = 35 mm, α = 0 and f = 15 cm.

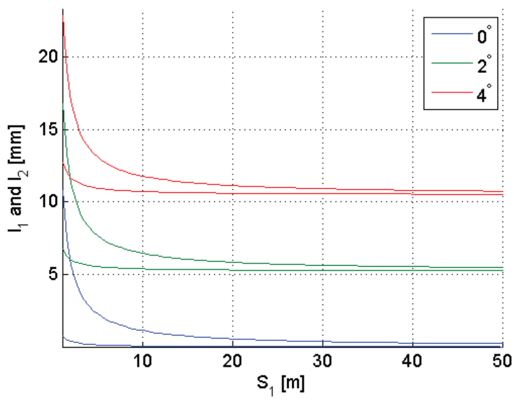

Figure 3.4: Simulations for testing laser spot in focal point when α is varied. r = 35 mm, a = 4 cm and f = 15 cm.

Chapter 4

Photodetectors

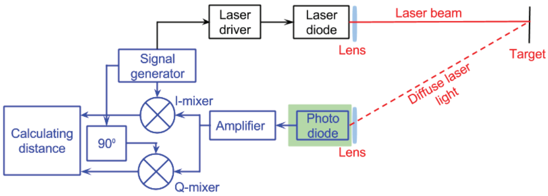

In this chapter the photodiode is discussed.

4.1 Introduction

At the beginning of the receiver chain, after any focusing and filtering optics but before the electrical processing stages, an element which converts the incident light, i.e. optical signal, to an equivalent electrical signal is needed. Ideally, this optoelectrical element would perform the conversion instantly, keeping the SNR, and produce an identical electrical copy of the signal suitable for amplification and further processing.

Sensors which convert optical power to electrical power, using the photoelectric effect, are called photodetectors. There is a variety of such devices available, each of them adapted to a specific application. Sadly, none of them exhibit the ideal properties described above. Instead, one needs to compare the different devices with respect to certain parameters in order to find the one best suited to the problem at hand.

Some concepts from semiconductor physics will be necessary to discuss the properties of different detectors, and these will be introduced as they are needed. However, since it is not the main topic of this thesis, it will be brief, and only meant to support the discussion and motivate certain decisions. Basic knowledge of semiconductor processing and devices, such as doping and pn-junctions, is assumed to be somewhat familiar to the reader.

4.2 Photodetector properties

To be able to compare different detectors one needs some way of measuring their performance. Below are some common properties by which photodetectors are characterized.

4.2.1 Photosensitivity

One of the most basic properties of a photodetector is its photosensitivity, which essentially describes its response when exposed to light, i.e. photons. This is usually given in units of A/W or V/W, i.e. amps or voltage per watts of incoming optical power depending on type of detector. Typically, photodetector sensitivity is not constant over the entire spectrum. This is why it is always quoted at a certain photon energy, or more commonly, presented graphically versus light wavelength. Thus the choice of detector depends on the wavelength of light which is to be detected, since it is often desirable to have peak photosensitivity at that wavelength. The photosensitivity is related to the quantum efficiency η of the detector, i.e. how efficient the photon-electron conversion is. [52]

4.2.2 Frequency response

Another basic property of a photodetector is its frequency response, or bandwidth (BW), and it describes the behavior of the device when the optical signal is time dependent. This may be specified in terms of cutoff frequency, f_T, or simply BW, in units of Hz, or as output signal rise and fall times, t_r and t_f. A fast detector has high f_T, which means it can better reproduce signals which vary fast in the time domain, than could a slow detector with low f_T. The frequency response depends on the underlying process by which light is converted, and may be altered by changing the operating conditions such as applied voltage. The manufacturing conditions may also affect the frequency response, since low standards typically yields low quality devices. Higher standards are reflected in better device performance, but also in the pricing.

4.2.3 Noise-equivalent power

All photodetectors produce noise when they operate. The amount of noise produced depends on the type of detector as well as on manufacturing and operating conditions. [28] This ultimately sets a lower bound for the detectable optical signal power, since when the level of the signal equals the level of the noise present in the system, it is not possible to distinguish between them, and only noise would be visible at the output.

The signal-to-noise-ratio, SNR, is a useful ratio for evaluating performance of components in a signal processing chain, and the situation just described can thus be expressed as having $SNR = 1$. It should be noted that the lower bound for signal detection set by the detector noise level may not be the limiting factor of the entire system. For instance, ambient light levels may be sufficiently high to drown the signal of interest, and the electronics following the detector may introduce noise causing a similar situation. It should be noted that this is not related to the internal noise in the diode, but rather external noise which will be discussed in section 7.5

The noise-equivalent power, NEP, of a detector is a measure of its sensitivity with respect to the minimum optical signal power at a certain wavelength and signal bandwidth it can detect. It is commonly defined as the optical power needed to obtain a signal-to-noise SNR = 1 at the output, and is then given in units of W/sqrt(Hz). [29] Thus, a detector with lower NEP should be able to detect weaker optical signals than a detector with higher NEP.

There are more parameters than the above mentioned ones which characterize a photodetector, but they are more specific to the physical process by which the detectors operate and will therefore be covered in section 4.3 where different types of detectors are discussed.

4.3 Photodetector types

As mentioned above there is a variety of photodetectors available. They span large intervals both performance-wise and cost-wise. In this section some common detector types are listed, and their properties and modes of operation are discussed.

4.3.1 Photodiodes

A photodiode is in its simplest form a pn-junciton in an elemental semiconductor such as silicon, as shown in figure 4.1. When a p-doped and an n-doped region are brought together, free charge carriers, electrons, supplied by the donor atoms in the n-doped region fill the empty states supplied by the acceptor atoms in the p-region, a depletion region with no free charge carriers is formed. The width of this depletion region depends among others on the n and p dopant concentrations, and the voltage applied to the junction. Using the Poisson equation [31] the electric field in the depletion region is calculated. From this the potential in the depletion region is calculated, and by switching sign, the energy, or band, diagram in figure 4.1 is obtained. An approximation typically used is that far away from the junction, the semiconductor is intrinsic.[30]

If the junction is forward biased, i.e. a positive potential is applied to the p-side relative to the n-side, the potential there is raised which causes the energy to lower. The barrier for charge carriers is then lowered, and a current can flow.

If however the junction is reverse biased, then that same barrier is instead raised, and no current can flow since there is no free charge carriers in the depletion region. The few free charge carriers which enter the region are swept away quickly by the electric field. Furthermore, under reverse bias, the width w of the depletion region increases, which decreases the capacitance of the junction.

For various reasons, electrons may be excited from lower energy states, such as the valence band, to the conduction band, where they can move to carry a current. Equivalently, one may consider this as an electron-hole pair being created. This may be due to sufficient thermal energy, or it may be caused by an incoming photon of equal or greater energy than the energy difference between the conduction band and energy state in question, be it the valence band or some dopant state. Naturally, the opposite reaction also occurs, where an electron enter a lower energy

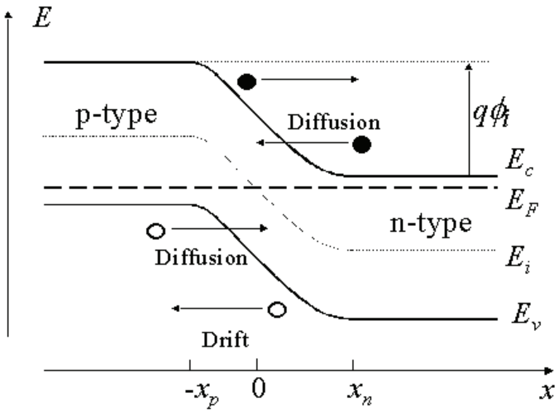

Figure 4.1: Band diagram of a Si pn-junction. E_c is the conduction band, E_v the valence band, E_i the intrinsic Fermi level, E_F the Fermi level, ϕ_i the built-in potential and $w = x_n + x_p$ the depletion region width. The arrows indicate charge carrier propagation due to drift and diffusion. [30]

state under the emission of a photon or phonon. Equivalently, an electron and a hole is said to recombine. The generation and recombination rates of electron-hole pairs are governed by equations which will not be further discussed here, but it can be mentioned that in equilibrium they are equal. [31]

In the presence of an electric field inside the depletion region, any free charges generated by e.g. illuminating the junction will be separated and swept away from where they were generated. This effectively stops them from recombining, resulting in a current whose magnitude depends on the amount of photons incident to the junction. This photocurrent is a rather linear function of the incoming light, and the frequency response may be quite fast, maybe in the MHz region. This configuration is called photoconductive operation, and it is the more suitable choice when a fast and linear response is required. [32]

The other configuration is called photovoltaic, and in this scheme the diode is unbiased. The response to illumination is instead a potential difference between the two terminals. This response is however slow, and not very linear. [32] It may present some advantage over the photoconductive mode, which will be discussed next.

In dark conditions, when there are no incoming photons, the photodiode should ideally be quiet. This is true for photodiodes in the photovoltaic mode, but in the photoconductive mode, there will be a small current called dark current present. The origin of this current are the charge carriers which diffuse into the depletion region from the p-side, and are swept away by the electric field. The dark current may thus limit the lowest level of light which can be detected, which is why it is advantageous to use a detector with as low dark current as possible. [32]

There are many ways to implement a photodiode and many parameters to tweak to optimize it for a certain application. While the simplest ones are elemental, e.g. silicon, pn-junctions, one may instead use compound semiconductors such as GaAs to vary properties of the diode. The bandgap of GaAs is 1.42 eV, while that for Si is 1.12 eV at room temperature, hence GaAs will be sensitive to other light wavelengths than Si. Furthermore, electronic properties such as electron mobility (9200 for GaAs and 1450 cm^2/V-s for Si) differ, and the generation and recombination rates may be different. [31]

There is also a fundamental difference between e.g. Si and GaAs, as Si has a so called indirect bandgap while GaAs has direct bandgap. This will not be further discussed here, but it is nevertheless mentioned as an important parameter for optoelectric devices. One may also combine different compounds to create heterojunctions, whose properties may be tailored precisely. Finally, one may also vary the doping concentration of the p- and n-sides.

4.3.2 The PIN-diode

It is not desirable to have recombination in the depletion region if the diode is operated in the photoconductive mode. Thus, to suppress recombination and to simultaneously favor electron-hole pair generation by increasing the area where this occurs, one option is to add an intrinsic layer between the p- and n-doped sides, where the majority of the electron hole pairs are generated. See figure 4.2.

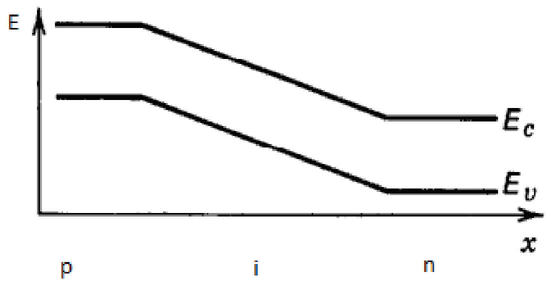

Figure 4.2: Band diagram of a Si pin-junction. Incoming photons generate electron hole pairs in the intrinsic region, which are then swept away by the electric field and cause the photocurrent. [33]

This structure is called a p-i-n diode, or PIN diode, named after the p-doped, intrinsic and n-doped areas. It is commonly used as a photodetector, and typically the performance properties discussed above are specified in its datasheet. The reverse bias needed to fully deplete and operate a PIN-diode is quite low; it may be around tens of volts, but for the ones used in this project 5 V is enough. The intrinsic region is very resistive, and so any voltage applied to the PIN diode will appear over this region.

4.3.3 The Avalanche Photodiode – APD

By increasing the reverse bias of a diode, one eventually reaches the breakdown voltage and the diode begins conducting a large current in the opposite direction. This is usually damaging for the diode and is with some exceptions an undesirable operation. However, by applying large reverse bias, typically 100-200 V in a Si APD diode, but remaining below the breakdown voltage, the diode may exhibit the so called avalanche effect which essentially provides internal gain, M, for the converted optical signal. The situation is illustrated in figure 4.3.

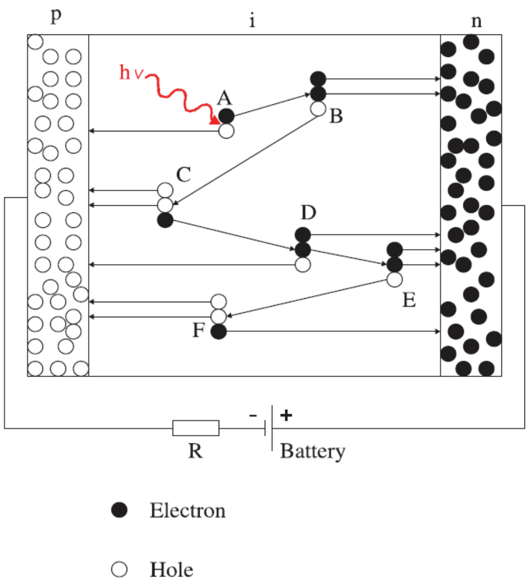

Figure 4.3: Illustration of Si APD operation. In the simplest case it is structurally the same as the PIN diode. Incoming photons generate electron hole pairs in the intrinsic region, which are then accelerated by the electric field. If this acceleration is large enough the charge carriers may excite new electron hole pairs when colliding with lattice atoms, creating the avalanche effect. [49]

When a large reverse bias is applied, the electric field strength in the depletion region may be as large as 200 kV/cm. Thus, when an electron-hole pair is created by an incoming photon, both charge carriers are accelerated. Statistically, the electron, and the hole, will collide with an atom in the lattice after one mean free path. When it does, it will transfer its energy, which is considerable due to the large electric field, to the lattice atom and effectively create another electron-hole pair.

This is called impact ionization. Both the original and the newly created electron will then be accelerated by the electric field, until they collide and then each electron will give rise to a new electron-hole pair, and so on. This very quick increase in current is referred to as the avalanche effect, and is what gives the internal gain. The diodes used as APD:s are optimized to have large breakdown voltages, since the larger reverse bias that can be applied, the larger the gain. [49]

The avalanche multiplication that gives the gain during APD operation also causes noise, and the amount of noise is specified as the excess noise factor F given in the component datasheet. This suggests that APD:s may exhibit much more noise than a PIN diode, which have no internal gain. This topic will be covered in section 7.5.3. Also, the reverse bias needed is typically much larger than for a PIN diode, which may cause practical circuit problems.

Another drawback with APD:s is that the gain is rather sensitive to temperature as indicated by the plot in figure 4.4 for the Hamamatsu S12023 APD used in this project. Depending on the application, it may be necessary to use a temperature compensated voltage supply for reverse biasing. Another alternative is to employ some thermoelectric cooling of the APD, which then keeps the operating temperature constant. Components with cooling integrated in the same package as the APD are available. [75]

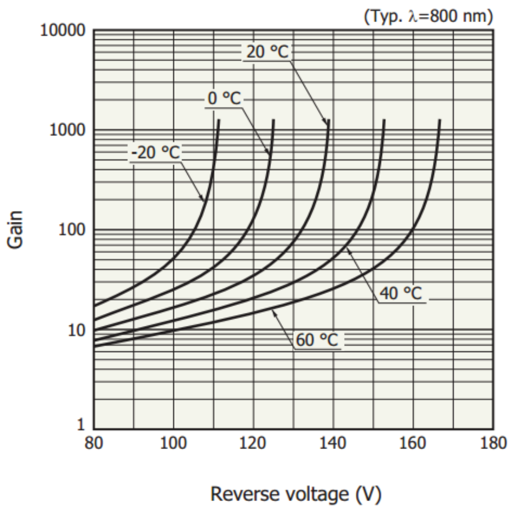

Figure 4.4: Plot of the APD gain for different ambient temperatures. To ensure stable operation one may consider employing cooling of the device. [74]

4.3.4 Photoresistors

A photoresistor is a device whose electrical resistance decreases as incident light intensity increases. They are based on semiconductors, either intrinsic or extrinsic, and their properties such as wavelength dependent sensitivity can thus be controlled. Incident photons with energies in a certain material dependent region excite electrons from the valence band to the conduction band, i.e. create an electron-hole pair, and these free charge carriers can then carry a current, which lowers the resistance of the device. [34]

Photoresistors are mainly used for detecting the presence of light rather than for performing accurate light level measurements. Their resistance may vary a lot with temperature, since the thermal energy available may cause excitation of electrons from the valence band to the conduction band, and thus increase conductivity. Furthermore they are typically slow devices, with rise and fall times in the ms range, and thus unsuitable for detecting high frequency signals. [35] The reason for this behavior is found in the relations that govern electron-hole pair generation and recombination rate, which will not be discussed further here.

4.3.5 Phototransistors

In its simplest form a phototransistor is a homojunction bipolar transistor (BJT) that has been optimized to work as a photodetector. This is done in part by increasing the size of the base and collector regions, since it is in the base-collector junction that the incoming photons generate the majority of the electron-hole pairs which constitute the base current. Since the phototransistor is biased the same way a regular BJT would be, i.e. with the base-collector junction reverse biased for an npn-BJT, the photocurrent is amplified by the current gain β. This may be on the order of up to a few hundred times for e.g. a Si BJT.

Much higher gains are possible using heterostructure phototransistors. Compared to an APD, the phototransistor produces much lower noise since there is no multiplication process involved. [36] However, the gain β of a BJT is typically very dependent on temperature and also on the device manufacturing process, and thus the signal processing may be complicated when using phototransistors.

The main disadvantage of homojunction phototransistors is that they are quite slow, i.e. have low f_T, typically not higher than 250 kHz. This is because of the large capacitance caused by the large base-collector junction, which is designed to be large to gather as much light as possible. Heterojunction phototransistors may have bandwidths of up to 1 GHz, but they are more expensive to fabricate and are therefore not widely available.

4.3.6 Photomultiplier tube – PMT

This is a class of highly sensitive and fast photoreceivers and they are often used in research to measure extremely low levels of light or even to register single photons. The device typically consists of a cathode, several dynodes and an anode suspended in some vacuum tube with an electric field applied. The incoming photons cause emission of electrons from the cathode, and these photoelectrons are accelerated by the electric field to the first dynode. This causes the emission of secondary electrons from the dynode, and these are accelerated to the second dynode, where more secondary electrons are emitted. After a certain number of stages, the signal will have been amplified, possibly as much as 10^6 times. Finally, the secondary electrons are collected by the anode, and the current is then the electrical copy of the optical signal. [37]

These detectors produce less noise than e.g. the APD which also has high gain, since there is no excess noise factor since no avalanche multiplication is involved.

However, due to their extreme sensitivity, care must be taken during experiments to ensure that they are not exposed to high levels of light. Just keeping a PMT out in the daylight may be enough to destroy it. Furthermore, they require a bias of about 500 V up to 1200 V DC to operate, which may be a practical inconvenience.

4.3.7 Charge Coupled Device - CCD

This type of photodetector is typically found in cameras and different imaging systems. Essentially, the sensor area is divided in smaller parts called pixels, and each pixel works as a small photodetector. During a certain amount of time, the pixels gather photons, and when the time is up, the number of electrons generated in the pixel by the incident photons is counted. This number is then related to the intensity of light at that pixel, and by using the contributions from all the pixels, an image of the scene is built up. [38]

These are typically large area detectors optimized for imaging, and they need calibrated focusing optics to perform optimally, as well as computational power to interpret the signal and create the image. They are therefore not well suited for detecting high frequency signals. For range finding applications, they may be used with the parallax method but they will not be considered for the homodyne receiver scheme. Possibly, the CCD sensor on its own could be used as detector, but this would require knowledge of how to properly interface to it, which the authors lack. It is therefore deemed to be beyond the scope of this project, but noted as an interesting notion given the amount of commercially available CCD sensors.

4.3.8 Arrays of detectors

Instead of using a single detector of the types mentioned above, there may be advantages of using several of them in some array. Advantages of this could be larger total active area or more flexibility in the PCB layout. There are also examples of dual detector setups, where one of them is receiving the signal and the other measures the background level and the outputs of these detectors are fed into a differential amplifier to cancel the background noise. [39] Depending on the configuration of the array, other problems such as large capacitance from the detector array may arise, and techniques to overcome this would need to be put in place. [52]

4.4 Selection of photodetectors

The basic requirements for the photodetector to be suitable for the homodyne receiver scheme are speed and sensitivity. Firstly, its sensitivity for the laser wavelength, i.e. around 650 nm, used must be reasonably high. Here reasonably means such that its peak sensitivity is in the vicinity of the laser wavelength, or around 0.4 A/W or equivalent. Secondly, its bandwidth must be sufficiently large, preferably in the hundreds of MHz, to be able to properly reproduce the modulated signal. Already using these two criteria, the photoresistor can be excluded as a candidate. They are simply not fast enough. For the same reason, the phototransistor can be excluded as well, since heterojunction phototransistors proved difficult to come by.

This leaves the photodiodes and the PMT. For practical reasons, such as the example above of PMT:s destruction by exposure to daylight, and the high voltage needed to bias them, PMT:s were also excluded. Furthermore, they are rather expensive at around 1000 USD. [40] As discussed before cost is not a crucial aspect of this project, but it is nevertheless desirable to design a system consisting of, in some sense, ordinary components, and PMT:s are not ordinary components. Thus the two detectors fulfilling all criteria so far are the two photodiodes, the PIN diode and the APD. Both types are available in many different packages with specifications ranging from ultrafast to large active area devices, with photosensitivities covering the entire visible and IR spectrum. Furthermore, they are represented in many different pricing ranges, from less than a dollar [41] to hundreds of dollars [42] per unit and beyond.

4.4.1 PIN diode and APD circuits

A receiver circuit using a PIN diode in the photoconductive mode could be made very similar to a circuit using an APD, since both diodes have a current response. Thus, the first amplifier stage would need to be a transimpedance amplifier in both cases. In fact, the only necessary difference between the circuits would be the diode bias circuit. As mentioned above, PIN diodes can usually operate on 5 V reverse bias, while APD:s may require 100 V or higher. It stands to reason that the PIN diode circuit will be easier to implement since no high voltage needs to be generated by e.g. a DC-DC converter with its associated temperature compensation circuit. Furthermore such high voltage requires more care to proper insulation when designing the PCB. Examples of these circuits and how they were implemented in practice is discussed in section 7.

4.4.2 Comparison of diode properties -NEP

Regarding the NEP, generally there is little difference between the two diode types, and for a typical device it has values between pico and femto watts per $\sqrt{Hz}$. This figure seems to be more related to price regardless of type, where higher price more often than not provide lower NEP. The higher price may reflect better manufacturing processes and quality controls than those for cheaper diodes, or simply imply a better performing device in general. This may in turn cause the lower NEP of more expensive devices.

4.4.3 Gain

As there are plenty of detectors of both types satisfying the bandwidth and photosensitivity requirements for our application, the remaining significant differences, apart from practical considerations, are the matters of gain and noise performance.

Since PIN diodes have no internal gain, a very weak optical signal would be converted to a very weak electrical signal at its output. This situation requires very low noise subsequent amplifier stages, as to not drown the signal in the noise generated by the amplifier itself. Also, high gains would be needed, which, depending on the modulation frequency, may be hard to obtain while maintaining sufficient bandwidth.

APD:s do have internal gain, which amplifies the signal and thus loosens the demands on subsequent amplifier stages. However, the noise is also amplified by the APD, and except for some special cases the SNR is not increased compared to the PIN diode. [51]

4.4.4 Noise performance

A more detailed discussion is provided in section 7.5, but an overview is nevertheless given here. Both diodes suffer from dark current, typically in the sub-nano amp range, which is the photocurrent when no light is incident on the active area. As in the case with NEP however, other factors than type of diode seems to affect the magnitude of the dark current. Again, higher price often suggests lower dark current, but also the band gap of the detector matters. A large band detector has lower dark current than a smaller band gap detector. [49] Also, operating conditions such as reverse bias may affect the dark current.

As mentioned above the APD also introduces more noise than the PIN diode due to the avalanche effect.

4.4.5 List of chosen photodiodes

This project aims to be a first study of the implementation of a certain laser range finder architecture. As such, one of its objectives is to map out important parameters and serve as a reference for future work. One parameter which is expected to impact heavily on performance is the photodetector, and for this reason not one but several photodetectors are considered and evaluated in this project. As mentioned before, within reasonable limits, neither cost nor the power consumption of the components are main concerns in this project. Following the previous discussion of different detector types, a total of three PIN diodes (Hamamatsu S10784 and S1223, First Sensor PS0.25-5t) and two APD:s (Hamamatsu S12023-10 and First Sensor AD100-12) were chosen for investigation. Together they cover a wide range of properties such as package, active area size, bandwidth and cost. They are listed in table E.1 in appendix E along with their main properties.

Chapter 5
Safety Aspects

5.1 Introduction

This project involves several potentially dangerous aspects, of which the risk of laser-induced eye damage may be the most prominent. The focus of this chapter is to explain the concepts and procedures for evaluating laser safety, and then to discuss their implications for this specific project. Laser classifications are discussed, and finally any other hazards, such as risk of electric shock, and the procedures to avoid them, are commented on.

As a rule of thumb, lasers in any form are dangerous, and no matter the output power one should never look directly into the beam. When handling a laser there are always safety aspects that must be taken into consideration. This is because at certain wavelengths even very low power lasers could damage the eyes.

The following discussion makes no assumption about the type of laser, i.e. the method for generation of the laser beam. This is instead the topic of section 3.2. Here a laser simply refers to a collimated beam of coherent and monochromatic light.

5.2 Laser safety

5.2.1 Laser classification

An essential part of this project is to emit and receive laser light. Intuitively, the higher optical power emitted, the more power is reflected of the target and can reach the detector, allowing for a higher SNR and an increase in the range of the device. However, depending on the application, the allowed output power of the laser may be limited.

One particular limiting factor is the risk of eye injuries, and to estimate this risk lasers in products are classified according to some standard. In this project the "American National Standard for Safe Use of Lasers", ANSI Z136 [24] standard is used, but it should be noted that there are several more or less equivalent standards worldwide. [25]

In this standard there are four classes, 1 to 4, including sub-classes. Somewhat simplified, the lasers in these classes range from low power and eye safe to high power and dangerous. Also, the viewing conditions and intended usage of the product may affect classification. See [24] for specific formulations and actual limits for each class.

The classes are based on eye safety during operation, and this is in turn based on what medical studies have shown to be dangerous exposure levels for eyes. Normally, any product which is to be commercially available should be classified by some authorized party to ensure consistent and reliable risk estimation for the end user application.

In this project the aim is to propose and verify a concept rather than to provide a finished product, and therefore formal classification of the lasers used is not meaningful. However, what is mandatory in this project, and always when working with lasers, is to evaluate the situation specific risk of eye or skin injury with the operators or any other person in the surrounding area during any given moment when exposure to the laser beam is possible.

Here laser classification may certainly be of help. For example, for a laser to be class 2 and thus eye safe under accidental exposure, which will be defined later, its output power must be below 1 mW. [24] Thus, if such a laser is used in the experiment, one can be sure of that accidental exposure will not cause significant damage.

Depending on the risk of eye injury using a certain laser, one may either decide to use protective eyewear, or choose to alter the project itself by switching to a safer laser. In any case, to evaluate the risk some concepts are needed, and they are introduced in the next sections.

5.3 Concepts and definitions

5.3.1 Structure of the human eye

In figure 5.1 an illustration of a human eye and its cross section with the major components marked are shown. In essence, the cornea and lens focuses the incoming light into an image on the photosensitive retina. This information is then transferred by the optical nerve to the brain for processing. The iris serves as limiting aperture for the incoming light, and finally there is the eyelid which may be controlled by the corneal reflex to stop light from entering the eye e.g. under exposure to very bright light. [43]

There are many ways that an eye can be damaged by exposure to a laser beam. The most likely type of injury depends on the wavelength of the laser, since for instance the eye reacts differently to visible and invisible light. Figure 5.2 illustrates how light of different wavelengths interacts with the eye. Generally, the risk for retinal injury is largest for visible and near infrared light. In this region the cornea is transparent, and thus the lens focuses the light onto the retina, where damage may occur depending on light intensity.

This is the primary risk considered in this project, since a visible laser of wavelength 650 nm is used. For longer and shorter wavelengths, the cornea and the lens respectively block the light. In this case the laser energy is dissipated there instead of on the retina, and thus either thermal or some type of photochemical damage similar to sunburn may occur. [43] As mentioned above there is also risk for skin damage, such as thermal burns, from laser exposure. This is however primarily a concern for high power lasers.

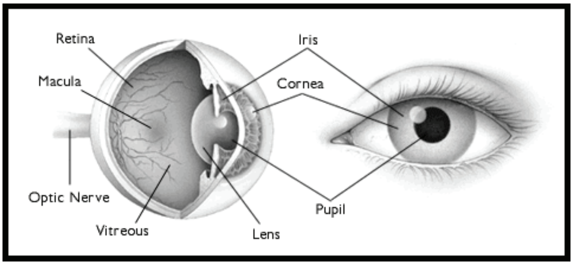

Figure 5.1: Schematic of the human eye. [43]

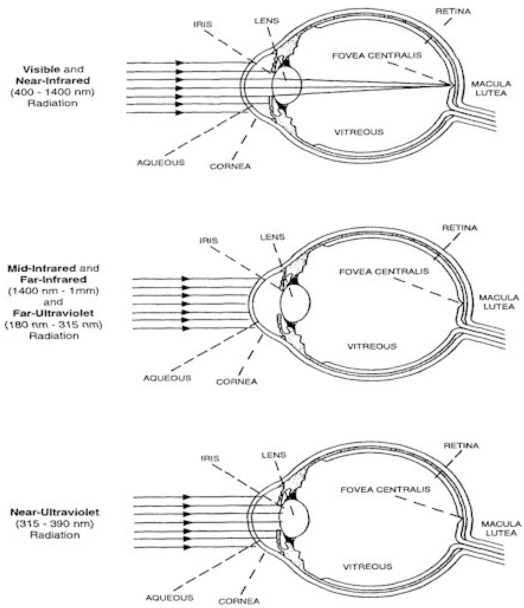

Figure 5.2: Ocular absorption site versus incident light frequency. [43]

5.3.2 Definitions, quantities and units

In the end it is the amount of light incident to the eye, the irradiance E [W/cm2] or radiant exposure H [J/cm2], that determines the risk of eye injury. These quantities may in any given situation depend on laser beam characteristics such as emitted power and beam divergence, or viewing conditions such as direct or reflective exposure of the laser light as well as viewing angle. In any case, the quantity used for eye safety calculations is the Maximum Permissible Exposure

(MPE). This is the maximum irradiance or radiant exposure that the eye can be exposed to without causing damage. The MPE is dependent on wavelength as well as exposure time, and formulas for calculating the MPE is tabulated in e.g. [24]

The Accessible Emission Limit (AEL) is another concept which is useful when a laser is to be classified. It defines the maximum output power of a laser in a given class.

Finally, there is the Nominal Hazard Zone (NHZ), which is the distance from the laser where the MPE is exceeded, i.e. where exposure to the laser light may be dangerous. Thus it depends on both wavelength and exposure time, and also on viewing conditions. The NHZ may thus vary depending on which exposure risks are present in the specific situation.

5.3.3 Reflectance

Typically, the laser beam may be viewed directly or reflected off some surface. In the latter case there are two variants, specular or diffuse reflectance. Specular reflectance is when the beam is more or less cleanly reflected off the surface, e.g. a visible laser beam being reflected off a mirror. The angle of incidence equals the angle of reflection.

Diffuse reflectance is when the light is reflected in all directions, approximately equally. The type of reflectance is dependent on the wavelength of light; for specular reflectance to occur the surface roughness must be small compared to the wavelength of light. Specular reflectance is thus potentially more dangerous than diffuse reflectance, since the radiant power of the reflected beam is much higher than the diffusely reflected light where the radiant power is spread out. [26]

5.3.4 Laser beam profiles

The above quantities also depend on the laser beam characteristics, particularly the spot size. The larger the spot size, the larger the area over which the radiant power is distributed and the less the irradiance incident on the eye. To get the correct value for the irradiance one must thus know the area, or limiting aperture D_f, over which the radiant power is distributed. As mentioned above the eye has a natural limiting aperture, the iris. When calculating the MPE for visible light, one uses the value $D_f = 7$ mm, as this is the diameter of a fully dilated pupil.

The above reasoning assumes that the laser beam has uniform irradiance across the diameter of the beam, and this is true for a so called top hat beam profile. The more common Gaussian profile however has a peak irradiance in the center, and its beam diameter a is instead measured at the point where the irradiance has dropped to 1/e relative the center. If however the beam diameter is similar to the limiting aperture of the eye, as in this project, one may use the top hat approximation and thus calculate the irradiance E_0 using equation 5.1 where ϕ is the radiant power of the beam and a is the 1/e beam diameter.

$$E_0 = 4\phi/\pi \cdot max(a, D_f)^2 \tag{5.1}$$

5.3.5 Exposure time

The MPE is dependent on the exposure time, and for evaluating eye safety in a certain situation, different values of this may be used. For deliberate staring into the beam, the exposure time is long and hence the MPE is low. Accidental exposure is precisely what it sounds like, and the actual time used depends on the visibility of the laser.

For visible lasers, it is 0.25 s which is the time it takes for the corneal reflex to advert the eye from the incident light. For invisible light, the time is instead 10 s, due to the lack of corneal reflex. If the exposure time is known, for example if a single pulse is emitted, this value may simply be used in the MPE formula.

5.3.6 MPE for pulsed operation

The above discussion assumes continuous wave (CW) output for the MPE calculations. If the laser is instead emitting pulses of light with some frequency, then the MPE calculations become more involved. Intuitively, the lower the frequency of the pulses the higher the power of each pulse could potentially be as the average power would be lower. As the pulse repetition frequency increases, it approaches continuous emission, and thus the power of each pulse would approach the MPE for CW emission.

This reasoning is valid with some restrictions, such as that pulse lengths below 1 ns is still considered to be 1 ns in the MPE calculations. The reason for this is the eye damage mechanism for ultra short laser pulses is different from that of longer pulses, and the approximation is used to be on the safe side. [24]

There are three rules for calculating the MPE for a pulsed laser, and the rule which gives the lowest MPE sets the MPE for the entire system. [4] The three rules are (1) the single pulse limit, (2) the average power limit and (3) the repetitive pulse limit. They are defined as:

(1) The MPE for any single pulse in the pulse train.

(2) The MPE for the maximum exposure time divided by the number of pulses n during that time.

(3) The single pulse MPE from (1) multiplied by $n^{-1/4}$.

The MPE for a each pulse in the pulse train must be lower than or equal to the lowest value given by the three rules above.

5.3.7 Procedure

The main concern is to determine if the setup is safe, so to this end the MPE of the laser is calculated under some assumptions based on the operating conditions, e.g. accidental or deliberate exposure. After this the irradiance incident on the eye is calculated using e.g. equation 5.1. Then these two are compared and the NHZ is calculated, or at least an estimation of the risk when low power lasers are involved is done.

5.4 Eye safety precautions employed

The initial experiments were to be carried out with a 5 mW output 650 nm laser, whose output is CW modulated. To simplify the risk assessment, it would be preferable to operate the laser so that its maximum output power is less than 1 mW. This number is calculated using the MPE, which in itself is based on the biological properties of the human eye as well as data from biological experiments on laser induced eye damage. [24] This output power would make it a class 2 laser, and thus safe for accidental exposure. The modulation could of course be set around a lower level, but to be able to emit safe levels without depending on the modulation circuit a ND2 filter was purchased. With this place in front of the laser beam, the power is attenuated by 75 %, rendering the output safe.

It was however discovered during experimenting that some practical matters such as focusing and actually detecting a signal was made easier with higher output power, i.e. without the ND filter.

This operation puts the laser in the class 3R instead, since the output power is limited to 5 mW. This of course poses a larger risk of eye damage, laser protective eyewear is usually not needed for this class if the exposure time is kept to accidental exposure only. [24] This suggests that diffuse reflections of the beam usually are not dangerous. The measurement setup was done so that a minimum amount of objects capable of specular reflection was in the laser beam path. By using diffusely reflecting blockades the laser beam was confined to the measurement area. See figures 5.3 and 5.4 for the setup. Furthermore, general care was exercised to avoid accidental exposure.

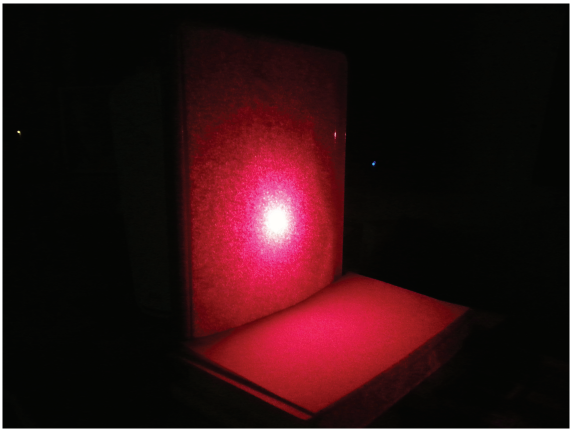

Figure 5.3: A white paper in the laser beam path serves as a diffuse reflector and prevents the beam from escaping the experimentation area.

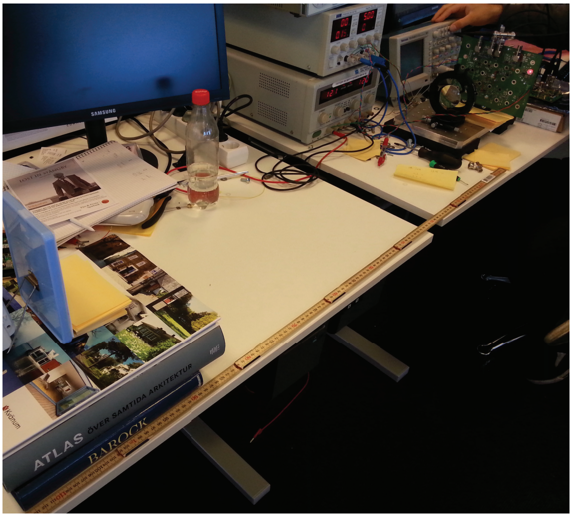

Figure 5.4: A second image of the measurement setup showing the blocking of the beam path by a diffuse reflector.

5.5 Other hazards

There are certain hazards while performing experiments on the setup which are not related to lasers. The most prominent of these is the risk of electric shock posed by the DC-DC converter which outputs around 200 V. Naturally, careful handling of the PCB when performing measurements is employed.

Chapter 6

Transmitter Circuit Design

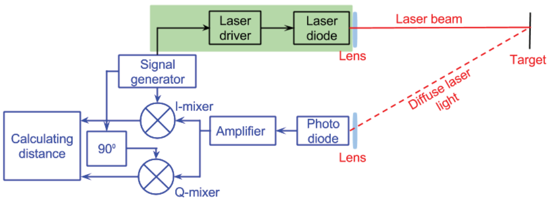

In this chapter the design of the transmitter is presented.

The most basic requirement of the transmitter block is to modulate the intensity of a continuous wave (CW) laser beam emitted from a laser diode (LD) at a certain frequency f_m. The driver circuit should allow for varying f_m over a wide range of frequencies fairly easy. It should also provide stable and low noise biasing of the LD, since these are sensitive components which may be damaged by exceeding their rated output power even for short amounts of time.

The authors chose to design their own driver circuit. The alternative to would have been to employ a commercial driver circuit, and some investigation into this was carried out. However, it was the authors impression that designing the circuit themselves would provide more flexibility which would allow for a greater variety of modulation schemes. The approach to modulate the LD bias current directly seemed to be sufficiently simple to implement, while simultaneously being an instructive task aimed to improve the authors' understanding of the system.

6.1 Driver circuit

The laser diode output power and drive current relation is highly temperature dependent which is shown in figure 6.1. The objective is to modulate the LD output power in the lasering region which corresponds to the high output power curve segments in figure 6.1. Operated below the threshold current level, the LD behaves as an LED, which is not desirable in this project.

LD:s are typically specified for a maximum output power, and if this value is exceeded, even momentarily, the LD may be damaged. It is therefore necessary to measure the output power, control the drive current and compensate for temperature fluctuations using a feedback loop. Many LD packages have a built-in photodiode which can be used for this purpose.

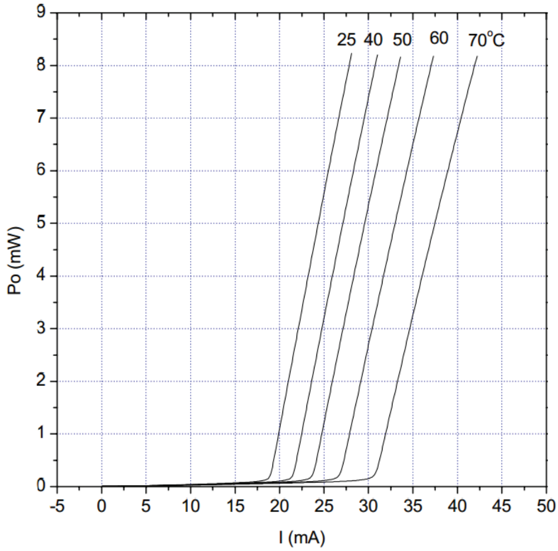

Figure 6.1: Example of output power versus bias current in the laser diode for differnt temperatures. [44]

The driver circuit that was chosen is shown in figure 6.2. Here $Vref$ controls the biasing point of the LD as it sets the voltage at the base of the transistor $Q1$, which together with $R1$ sets the current. Thus $Q1$ and $R1$ acts as a transconductance stage, and they limit the LD drive current by local feedback. The feedback is provided by the op amp and $R2$. $C1$ provides a path for the modulation signal to bypass the feedback loop, since it is only the bias point which should be controlled. $R3$ is a small resistor to prevent any oscillation in $Q1$, and $R5$ is a 1 kΩ resistor to measure the photodiode monitor current. The modulation is provided through the $inputMOD$ pin and is AC coupled with $C2$. [45]

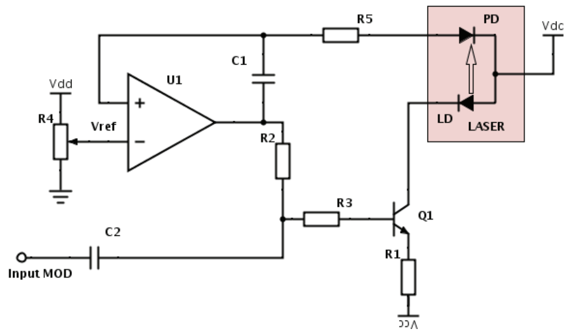

Figure 6.2: Illustration of the chosen laser driver circuit.

A 650 nm LD with maximum output power of 5 mW was chosen, satisfying the visibility and eye safety conditions previously discussed. The op amp and the transistor have to have sufficient bandwidth and low noise. The chosen parts are listed below.

- Laser diode $ADL-65055TL$ [46]
- Op amp $AD8021$ [47]
- Transistor $BFR93A$ [53]

6.1.1 Simulation

An LTSPICE model of the driver circuit was made. Models for all the parts except for the laser diode were available. For the laser diode a custom model was instead created based on the output power drive current relation data from the datasheet in question. This model is presented in appendix B.

A DC analysis was first set up to determine a suitable biasing point $Vref$ and to tune the component values for desired DC characteristics. The simulation result is presented in figure 10.1.

Secondly, a transient analysis was performed at the selected biasing point and component values were fine tuned for optimum AC characteristics. The minimum considered frequency was 10 kHz and the circuit was optimized to allow for as large modulation frequencies as possible.

Both sine and square waves were used as input signals during simulation, but for square waves the maximum frequency achieved without excessive distortion was 10 MHz. The resulting wave forms from the simulations are shown in figures 10.2.

Chapter 7

Receiver Circuit Design

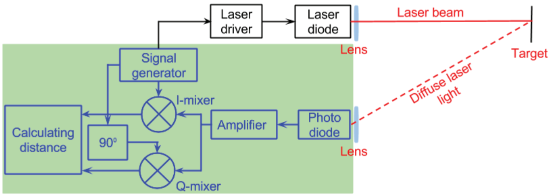

In this chapter the receiver block is designed.

As the name suggests the objective of the receiver circuit is to receive the diffusely reflected laser light, convert this light to an electrical signal and then amplify it to suitable levels. Furthermore it should also measure the phase difference between this signal and the transmitted one with some specified accuracy.

This does indeed place many constraints on the circuit design, and in this chapter the chosen circuit topology is described and evaluated. The receiver response time is investigated using simulations, and finally its noise performance is investigated.

Two different designs were produced in this project. The second design is the result of improving the first design with respect to the discovered shortcomings, and adding some functionality. The first design is shown and discussed in Appendix A, while the second design is considered the main design of the project and is the one all following discussion is based on.

7.1 Amplifier chain

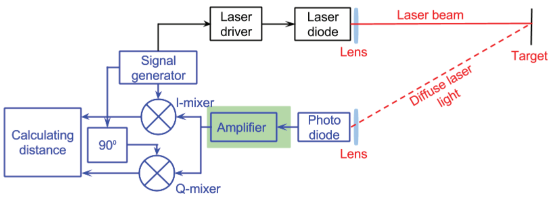

In this section the amplifier block is designed.

The discussion in this section assumes that there is an electrical signal from the photodiode present. To amplify it, one or more amplifier stages may be used. Two amplifier stages were considered since sufficient gain was not achieved with only one stage. As discussed in section 7.3, A third amplifier is present on the demodulation board.

7.1.1 Front-end amplifier

The front-end amplifier converts the current signal produced by the photodiode to a voltage and amplifies it. Such an amplifier is called a transimpedance amplifier (TIA). Since this is the first stage in the receiver chain its noise should be very low as this will be the main contributor of noise according to Friis formula. [55] Therefore the $ada4817$ [69] which is a low current noise (2.5 fA/$\sqrt{Hz}$) op amp with sufficient bandwidth is chosen. A convenience with this op amp is that it has a feedback pin close to the input pin, which can be used to reduce the physical length of the feedback loop.

A simple TIA circuit is shown in figure 7.1, where I_{diode} and C_{in} models the photodiode current and the combined diode and op amp input capacitance respectively.

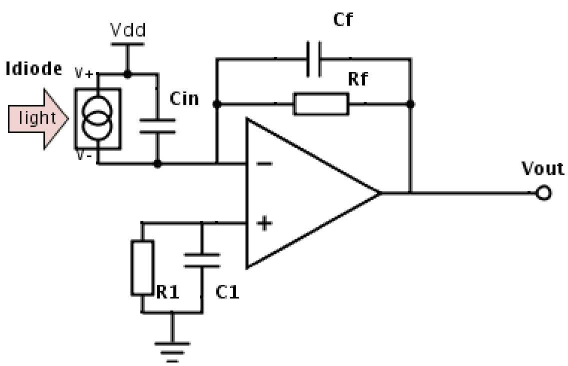

Figure 7.1: Schematic for the transimpedance amplifier.

DC analysis

To avoid any DC voltage amplification, $R1$ should be equal to R_f. This condition thus removes any DC offset at the output.

AC analysis

Considering again 7.1, $C1$ provides an AC ground on the non-inverting input and shorts out the noise from $R1$. The transfer function for this circuit is shown in equation 7.1.

The gain is set by R_f and the bandwidth is limited to $C_f R_f$. The reason for adding C_f in parallel with R_f is to introduce a pole in the transer function to avoid instability, and will be discussed next.

$$\frac{V_{out}}{I_{diode}} = \frac{R_f}{1 + sC_f R_f} \tag{7.1}$$

The feedback factor, $1/\beta$ is calculated in the same way as for a voltage amplifier by first considering the open loop case, see equation 7.2. The open loop gain is given by $A = f_{GBW}/f$ where f_{GBW} is the 0 dB gain frequency of the op amp. If the compensation capacitor is not applied, then $C_f = 0$, and thus both the zero introduced by $1/\beta$ and the pole introduced by A will result in a phase shift of 90°. The total phase shift will then be 360 ° since the amplifier gives 180° phase shift when its inverting input is used. Since $1/\beta$ has a slope of $+20$ dB and A a slope of -20 dB there will be a point f where $A\beta = 1$. See figure 7.2 Oscillation will then occur since both parts of the Barkhausen stability criterion is fulfilled. [59]

$$1/\beta = \frac{V_{out}}{V_{in}} = \frac{1 + sC_f R_f}{1 + s(C_{in} + C_f)R_f} \tag{7.2}$$

To avoid instability, the capacitor C_f with a suitable value is added which introduces a pole keeping the phase shift below 360°. To be on the safe side, a large value of C_f may be used. This will however limit the bandwidth. Decreasing the value of C_f increases bandwidth, but there is a greater risk of instability.

To maximize bandwidth without risking instability, the pole at $f = 1/2\pi C_f R_f$ should be placed at the frequency where $A = 1/\beta$. This implies solving the equation $A\beta = 1$ for C_f. The simplified expression is shown in equation 7.3. By assuming that $C_f << C_{in}$ then this expression can be further simplified and its solution is shown in equation 7.4.

Putting C_f at exactly the calculated value means being on the edge of instability, which may cause problems with ringing. This could be avoided by overcompensating, but again, this reduces the bandwidth. [58]

$$1 + \left(\frac{C_f + C_{in}}{C_f}\right)^2 = 2(2\pi f_{GBW} R_f C_f)^2 \tag{7.3}$$

$$C_f = \sqrt{\frac{C_{in}}{2\sqrt{2}\pi f_{GBW} R_f}} \tag{7.4}$$

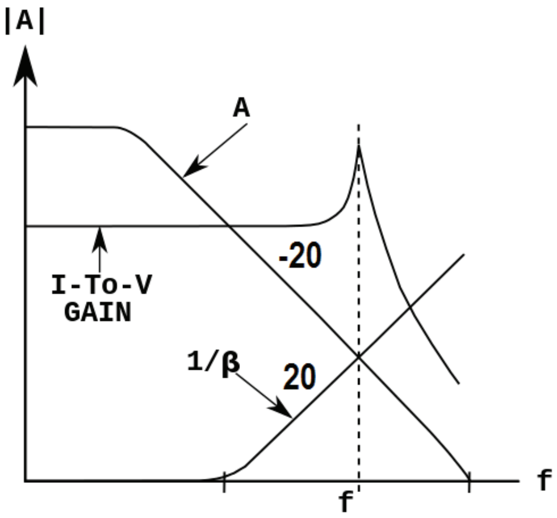

Figure 7.2: Illustration of the open loop gain and the feedback factor of the uncompensated TIA. [60]

7.2 Second stage amplifier

As mentioned above, not enough gain is achieved in the first stage amplifier. Especially not since the compensation capacitor C_f needs to be added which limits the bandwidth further. A second stage amplifier is needed, and here its noise performance is not critical, as explained by Friis formula [55], but it is still preferable to use low noise parts as the signal is still weak. A simple inverting amplifier scheme with a low voltage noise (0.85 nV/$\sqrt{Hz}$) op amp,$OPA847$ [56], was chosen, see figure 7.3. This scheme amplifies the signal by the ratio $G = R_f \ / \ R_g$.

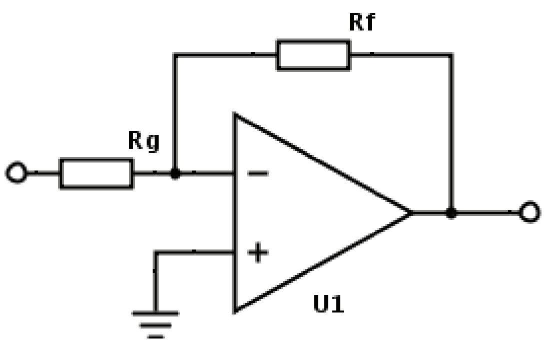

Figure 7.3: Schematic for second stage inverting amplifier.

7.2.1 Simulation

The entire system was modelled and simulated in LTSPICE. Figure 10.4 shows an example of the result of one such simulation, where the amplification of the system is plotted versus frequency. As mentioned before, higher feedback resistor in the TIA gives higher gain but lower bandwidth, and a higher feedback ratio in the second stage gives higher amplification.

7.3 Demodulation

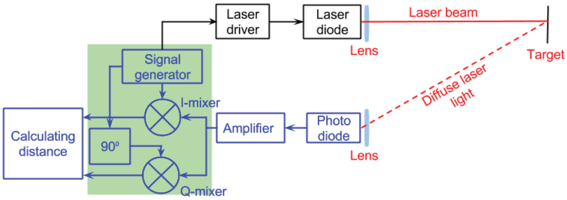

In this section the IQ-demodulator is discussed.

An IQ-demodulator IC (AD8333) was used for phase shifting and mixing. This part came mounted on an evaluation board with a fully differential amplifier (AD8332) on the input and a 90 kHz active low pass filters on the I and Q outputs[68]. The demodulator required 4 times the LO frequency as LO input and the detected and amplified laser modulation frequency as RF input.

To generate the required signals, the RF = LO frequency signal to the laser driver circuit and the 4 x LO signal to the demodulator, the square wave output of a 100 MHz crystal oscillator was fed to a binary counter (74VHC4040M) [70]. The binary counter then divided this signal by 2 in order to obtain the required 4 x LO signal at 50 MHz, and by 8 to obtain the LO signal at 12.5 MHz.

7.4 System simulation

To verify the receiver architecture system level simulations were performed using Agilent Advanced Design Software (ADS), see figure 7.4 for the schematic used. Ideal models of mixers, amplifiers and filters were used. Channel loss and other noise contributions were not considered initially, thus actual signal power levels were not of importance. The phase shift introduced by travelled distance was modelled by a simple time delay block.

Transient analysis was done to verify correct behaviour of the receiver. The result of one such simulation is shown in figure 7.5. Here the responses of the I and Q mixers are shown. Performing the calculations presented in section 2.1 using the stationary values of I and Q in figure 7.5, and comparing this to the period time of 1 μs of a 1 MHz signal, this phase difference of around 71.1° corresponds to a time difference of 0.1975 μs, i.e. the time delay introduced by the channel model, allowing for some error reading values in the graph. This result suggests that the receiver architecture works in theory.

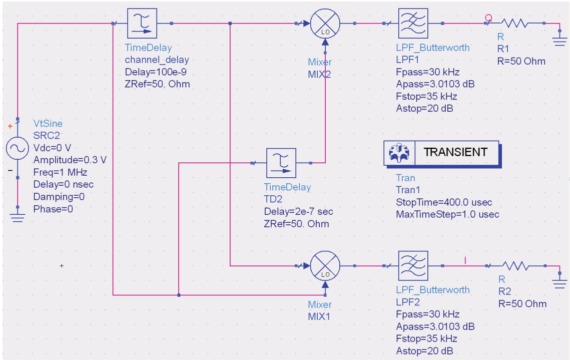

Figure 7.4: The schematic used for the system simulations in ADS. Here the the models are ideal, and no channel loss is taken into account. A 1 MHz sine wave is applied to the lossless channel.

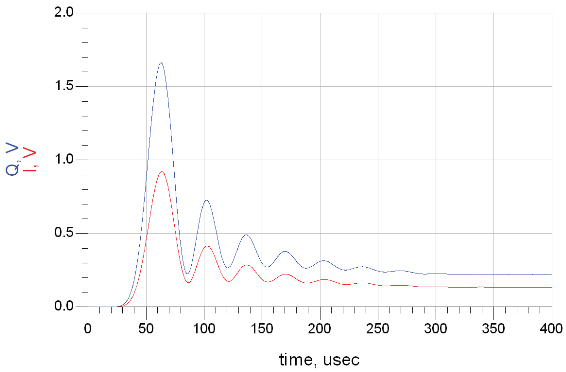

Figure 7.5: The result of a transient analysis. The channel delay is set to 0.2 μs corresponding to a phase difference of 72° and the output filter cut-off frequency is set to 90 kHz .

7.4.1 Receiver response time

Every time the distance changes the phase difference between the transmitted and received signal changes, and the effect of this can be modelled as a unit step signal being applied to the receiver. The response time of the receiver, i.e. how fast its response can give a correct, with respect to some given value, phase difference after applying a unit step, and thus how many measurements per unit time it can perform, is given by its step response. The transient analysis result presented in figure 7.5 shows the system step response for certain parameter values. In this case the I and Q values seem somewhat stable after about 80 μs.

By increasing the filter corner frequency to 850 kHz, another step response is obtained and is shown in figure 7.6. Here the I and Q values are stable after about 10 μs, but as can be seen the output now oscillates more strongly before the stationary value is reached. There is thus a larger uncertainty in the I and Q values for smaller times, which translates to a distance measurement uncertainty.

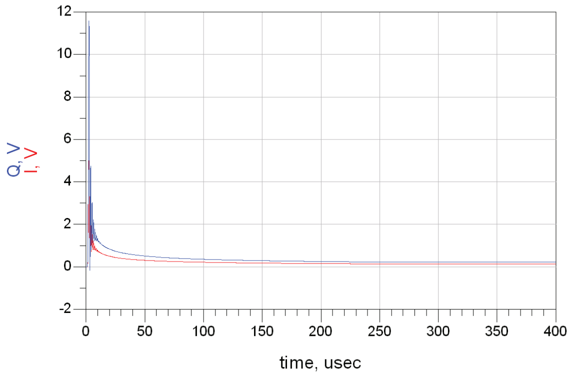

Figure 7.6: The result of a transient analysis. The channel delay is set to 0.2 μs and the output filter corner frequency is set to 850 kHz.

Decreasing the filter corner frequency to 10 kHz gives that the I and Q values are somewhat stable first after about 250 μs as shown in figure 7.7. Now there is less oscillation around the stationary value resulting in less uncertainty, but in turn it takes longer time to reach this value, i.e. the receiver is slower than before.

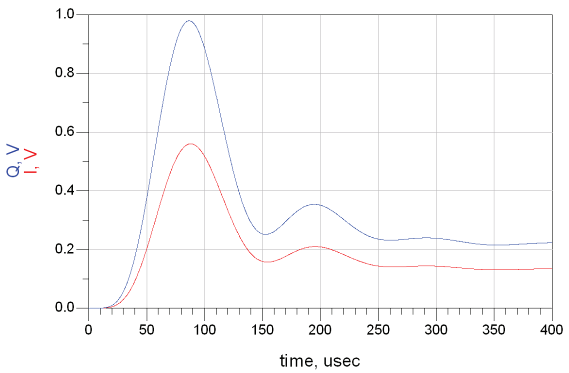

Figure 7.7: The result of a transient analysis. The channel delay is set to 0.2 μs and the output filter corner frequency is set to 10 kHz.

In conclusion the speed of the receiver is set mainly by the output filter corner frequency. The actual value is expected to be a trade-off between the specified system response time and desired measurement accuracy. Certainly, in a further developed device one would perhaps like to employ an ADC to be able to process the measurement values and use them for some application. In these cases one must ensure that the ADC is fast enough to not limit the receiver.

7.4.2 Noise simulation

Attempts were made using Harmonic Balance to simulate noise in the system by adding noise sources in the schematic. The channel loss was also modelled. The objective was to find the performance limiting stages in the complete system, and then use this as a guide as to where extra care should be taken during hardware design. However, difficulties modelling the system in combination with time constraints lead to inconclusive simulation results, and these are therefore omitted.

7.5 Noise considerations

The performance of the system presented up to this point will eventually be limited by noise. There are many sources of noise present, for instance ambient light conditions, noise from the electronics in the receiver and shot noise from the photocurrent from the photodiode. It is important to map out the noise sources present in the system, estimate the affect on performance they have and then try to design the system for minimizing the effect of the most significant ones. The signal-to-noise ratio, SNR, is a useful concept for evaluating performance at different stages in the system.

When designing a system such as this trade-offs between bandwidth, sensitivity and SNR are inevitable. There are however techniques for avoiding trade-offs to some extent, especially concerning SNR and bandwidth, which will be discussed in this section. [48]

7.5.1 Noise modelling

To estimate the noise in the system some models for the noise sources needs to be applied and analysed. The PIN diode and the APD are treated separately as they differ some regarding noise analysis. The following discussion of how to improve noise performance and bandwidth applies to both types of detectors.

7.5.2 PIN diode and TIA system

In section 7.1.1 the photodiode was modelled as an ideal current source with a parallel capacitance which represent the photocurrent I_d and the junction capacitance C_d respectively. There are several sources of noise in the simple PD and TIA pair, and they are shown as current or voltage sources in figure 7.8.

First, i_{Namp} is the input current noise of the op amp, and it is specified in the datasheet, and so is its input voltage noise e_{Namp}. As discussed in section 7.1.1 the input voltage noise is amplified as in equation 7.2, causing a noise gain peak which may cause instability unless C_f is added.

The feedback resistance R_f has thermal noise, and this appears as a current source i_{Nth} parallel to the photocurrent I_d. It is given by the equation 7.5, where k

is Boltzmanns constant, T the asolute temperature and B the electrical bandwidth of the photodiode.

$$i_{NTh} = \sqrt{\frac{4kTB}{R_f}} \tag{7.5}$$

The final current noise source is i_{Ns}, and this is the shot noise of the photocurrent I_d. It is given by the equation 7.7, where q is the electronic charge. The photocurrent however consists of three components where I_{Signal} is the current due to the signal, $I_{Background}$ is the current due to the ambient light and I_{Dark} is the dark current of the diode. [49]

$$I_d = I_{Signal} + I_{Background} + I_{Dark} \tag{7.6}$$

$$i_{Ns} = \sqrt{2qI_dB} \tag{7.7}$$

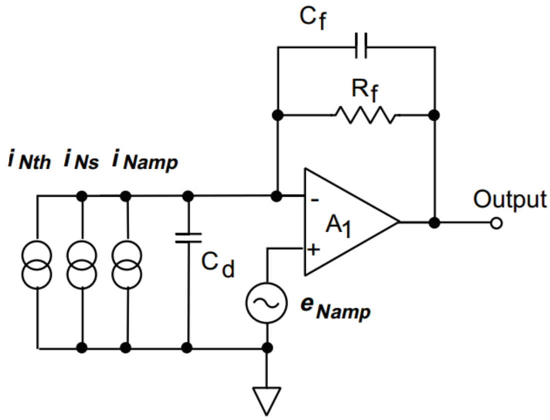

Figure 7.8: Schematic showing noise sources in the PIN diode and TIA system. [48]

In summary, since the noise sources discussed above are not correlated, the SNR of the PIN diode and TIA system can be written as

$$SNR = \frac{{I_{Signal}}^2}{{i_{Ns}}^2 + {i_{Namp}}^2 + {i_{Nth}}^2} \tag{7.8}$$

7.5.3 APD and TIA system

Much of the discussion of the PIN diode applies to the APD as well. In fact, figure 7.8 can be used to model the APD situation, if the internal gain M and the excess noise factor F is taken into account. The photocurrent I_d consists of the same components as in equation 7.6, but the shot noise of I_d is now instead given by equation 7.9 where M and F are defined as above.

$$i_{Ns} = \sqrt{2qI_dBM^2F} \tag{7.9}$$

Noting that the current due to the signal I_{Signal} is now multiplied by the gain M, the SNR of the APD and TIA system can therefore be written as

$$SNR = \frac{{I_{Signal}}^2 M^2}{{i_{Ns}}^2 + {i_{Namp}}^2 + {i_{Nth}}^2} = \frac{{I_{Signal}}^2 M^2}{2qI_dBM^2F + {i_{Namp}}^2 + {i_{Nth}}^2} \tag{7.10}$$

Thus, the APD provides higher SNR than the PIN diode when the noise is dominated by thermal noise i_{Nth}. [51]

7.5.4 Improving noise performance and system bandwidth

As discussed in section 7.1.1, the diode capacitance C_d, appearing in parallel with the op amp input capacitance C_{in}, together with the feedback resistor R_f causes a noise peak which limits the amplifier gain that can be used. A photodiode with larger capacitance would limit the bandwidth more than one with lower capacitance for a specific gain. Thus, it is desirable to reduce the effect of the photodiode capacitance on the system and thus simultaneously achieving higher bandwidth.

One way of doing so is to connect a BJT in common-base configuration to the input of the op amp as shown in figure 7.9. This is called a cascode, and what it does is essentially to isolate the op amp input from C_d by working as a current buffer. The photodiode is connected to the emitter of $Q1$, which in this configuration transmits the emitter current to the collector while keeping the emitter voltage constant. This potentially allows for larger bandwidth since the photocurrent now sees the small signal resistance of the emitter, r_E, instead of R_f. Furthermore, since C_d is isolated from the op amp input as $Q1$ acts a current buffer, one can increase R_f to reduce its thermal noise as per equation 7.5. [48]

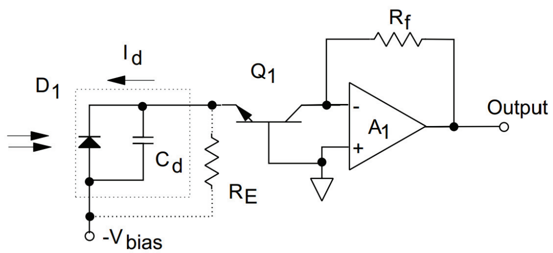

Figure 7.9: Schematic showing the cascode configuration intended to improve noise performance and bandwidth. [48]

A drawback with this configuration is that the collector current, entirely comprised of the photocurrent, can be shown to have full shot noise for all frequencies. [48] Two possibilities for increasing the bandwidth and reducing the shot noise of the collector current are external biasing and so called bootstrapping.

External biasing is simply adding a bias current to the photocurrent, which causes r_E to decrease and thus increasing the system bandwidth. The lower impedance of the emitter causes the collector current shot noise to decrease, as it is proportional to the square root of the collector current. The higher the bias current the larger the benefits, but the main limiting factor is the shot noise of the base current. It can be shown that the external bias current is limited by the base shot noise to a factor of $1/\beta_0$ of full shot noise, where β_0 is the DC current gain of the transistor. Thus large β_0 transistors may offer an advantage.

Nevertheless, when the limit is reached, bootstrapping is the better option. The schematic in this case is shown in figure 7.10. Here a second BJT is added in the common-collector configuration. Assuming that this transistor has a large DC current gain β_0, the voltage gain from base to emitter is approximately unity, essentially forcing the voltage drop over C_d to be constant.

Since the bootstrap has much lower impedance than the cascode, r_{E1} of $Q1$ is replaced by r_{E2} of $Q2_m$ due to $I_{c2} >> I_{c1}$ which increases bandwidth. Furthermore, since it removes the capacitive loading on $Q1$, it effectively removes the effect of the $Q1$ voltage noise.

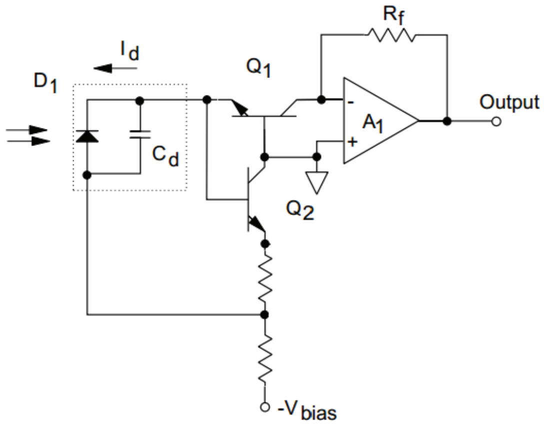

Figure 7.10: Schematic showing the bootstrapped cascode circuit intended to improve noise performance and bandwidth of the system. [48]

7.5.5 Other measures to reduce noise

A typical Si photodiode such as those used in this project are sensitive to the entire visible spectrum and beyond. Thus the ambient light, i.e. background power, is a source of noise when performing measurements. In the best cases, the ambient light would simply cause a DC offset at the detector output, which could be simply filtered away.

However, in some situations the ambient light may be sufficient to saturate the amplifier, rendering it impossible to discern the signal. Furthermore, by equation 7.7 it is clear as $I_{Background}$ increases, so does the shot noise of the photocurrent.

By equation 7.8, this also causes a decrease in SNR. Even worse, there are indications that due to the nonlinearity of the photodiode, there will be mixing of the signal with the background field, which introduces even more noise. [50]

To avoid this situation, it is advisable to insert a narrow optical bandpass filter in the signal path just before the photodetector. There are even photodetectors which have such a filter already mounted on the package. [73] Other methods of reducing noise from ambient light may be to cover the measurement device with some light blocking textile, or to simply perform measurements in low ligth conditions.

Depending on if the system is limited by shot noise or by thermal noise, it may be an advantage to actively cool the detector. As mentioned in section 4.3.3 keeping an APD type detector at a constant temperature keeps the gain constant. This mainly helps keep the system behaving more predictably.

Cooling a Si PIN diode may not help much with noise. This is due to the relatively large bandgap of 1.11 eV at room temperature. Electrons have around kT =0.025 eV thermal energy at room temperature, so there is little chance of electrons being excited to the conduction band in room temperature. [52]

Chapter 8

Implementation

To implement the system it was decided that a PCB was to be produced directly, without prototyping on a breadboard first. The reason for this was that such a prototype would simply not suffice with respect to signal integrity, considering the small signal levels predicted in chapter 3. Also, the parasitic capacitances at the frequencies in question would be too large. The schematic and PCB layout was performed in the computer program DesignSpark PCB.

8.1 Schematic

For the circuit design, the components and circuits were added and connected as described previously in chapter 6 and 7. Additionally, the following was done:

- Decoupling capacitors with values of 100 nF and 1 nF were added to the power supplies of each IC. Also a 10 μF capacitor was added for each voltage source.
- To reduce noise from the power supply an ultralow noise voltage regulator (adm7150) was used [71] for the positive supply and a low noise voltage regulator (LM2990S) for the negative supply [72]. A separate adm7150 was used for the photodiode to avoid noise leakage from the the rest of the circuit via the power supply.
- In order eliminate the risk of connecting the power supply incorrectly, reverse polarity protection transistors were employed. For the positive supply a pmos transistor was used and for the negative supply an nmos transistor was used. [57] In both cases the drain was connected to the PSU and the source to the voltage regulator outputs, while the pmos gate was grounded and the nmos gate connected to $+V_s$. See figures 8.1 and 8.2 for schematic.
- Where variable voltage was required, 1 kΩ SMD potentiometers were used.
- The signal generator blocks were connected with 0 Ω resistors to allow for easy selection of different frequencies. They were connected both to the transmitter and the receiver blocks, since the signals were needed in both these subsystems.

- Each of the different photodiodes described in chapter 4 were equipped with an individual TIA stage to minimize the trace length between the diode and the TIA. The outputs were then connected through 0 Ω resistors to the second stage amplifier common to all detectors for easy selection of photodiode.

- To provide the high bias voltage needed for the APD:s, a $R12-150B$ DC-DC converter was used [66].

- To avoid loading of the signal generators, buffer amplifiers were added to the phase shifter circuit and the I- mixer since their input impedance is low.

- A possibility to add a bootstrapped cascode on the TIA input was added, see section 7.5.4. It was connected with 0 Ω resistors to allow for easy connection and disconnection.

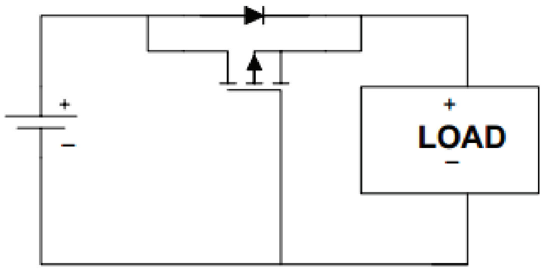

Figure 8.1: Schematic of the reverse polarity protection where a PMOS is used for the positive supply. [57]

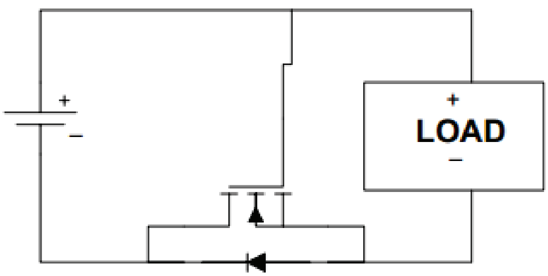

Figure 8.2: Schematic of the reverse polarity protection where an NMOS is used for the negaitve supply. [57]

The entire schematic is shown in figure 8.3.

8.2 Board layout with CAD

In this project a two layer PCB with 35 μm copper and 0.8 mm FR-4 substrate with dielectric constant of 4 was used.

To reduce the length of the signal path, male SMA connectors were placed on the back side of the board with the same spacing as the female SMA connectors on the evaluation board to allow for direct mounting.

The components were added from the schematic and placed in a logical order on the PCB. The decoupling capacitors were placed as close as possible to the components they were intended to decouple. Large vias with suitable diameters were added with 25 mm spacing to facilitate PCB mounting on an available optical bench.

To minimize reflections 50 Ω traces were used wherever possible. The widths were calculated with an online trace impedance calculator [67] to be 8 mm. Signal trace length was minimized. Ground planes with 0.2 mm trace isolation were added on both the top and bottom layer.

The top layer was used for components and routing as much as possible to maintain a unbroken ground plane on the bottom layer. Vias for connecting the top and bottom ground plane were placed where possible in a 3 mm grid., especially around the components that were connected to ground. The entire layout is shown in figure 8.3.

Three different positions were made for the LD to accommodate for different lenses and still be as close to the detector as possible, see section 3.2.1.

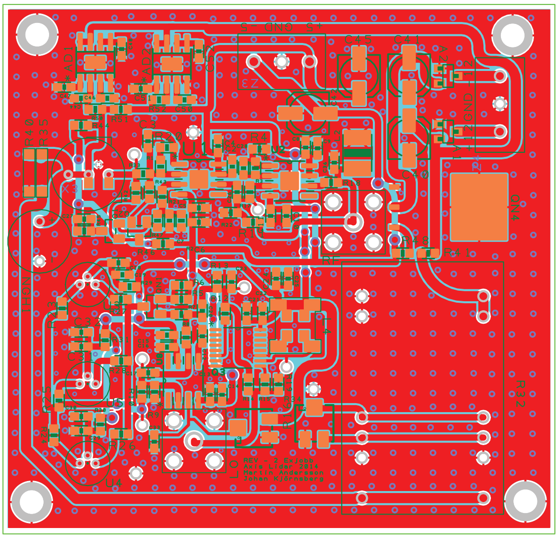

Figure 8.3: PCB layout.

8.3 Mounting

The components were soldered onto the PCB according to the schematic. Every time a power consuming device was mounted the power was connected to test for failures or bad solder joints. The board was then mounted vertically on an optical bench with the capability to move the board in the x-,y- and z-directions. In front of the photodiodes a lens holder was placed, where one of the three lenses at a time was mounted. A holder for the collimating laser lens was constructed to focus the laser beam. The board was connected to a ± 5 V supply.

Chapter 9

Experimental details

In this chapter the methodology for testing different parts of the circuit is presented. This includes a description of simulations performed on the circuits, as well as the measurement setup when performing physical experiments. Some countermeasures employed to eliminate some noise sources are discussed.

9.1 Function test

Some basic function tests of the realised system are needed to verify correct behaviour and to ensure stability of operation. This is important when performing measurements, since it is preferable to obtain reliable and reproducible results. In this section the tests performed on each block is described.

9.1.1 Transmitter circuit

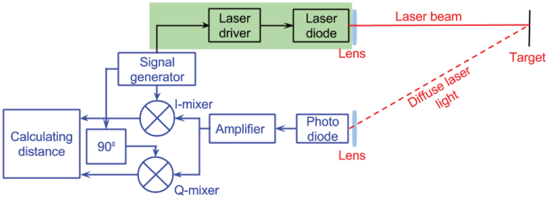

In this section the function test of the transmitter circuit is presented.

A DC analysis of the transmitter circuit was performed by increasing V_{ref} from 0 V to 12 V with more measurement points in interesting regions. Simultaneously measured was V_{in} and the voltage drop over $R5$ to measure the monitor current, see figure 6.2. These measurements were carried out with a FLUKE 115 True RMS multimeter. The results are presented in figure 10.1.

To test that the laser driver in fact modulated the laser light, signals with frequencies up to 100 MHz were applied to the input of the driver circuit. The monitor current was then measured with a Tektronix TDS 2024B digital storage oscilloscope (DSO) by putting one probe on each side of $R5$. The monitor current was then measured by taking a 128 point average of the difference with the oscilloscope math function. The results for a 12.5 MHz triangle wave as input signal is presented in figure 10.3.

The photodiode and TIA block output was measured with a DSO probe while the light levels were changed. To change the light level a white LED lamp was used to illuminate the photodiode. When the light level was changed the corresponding voltage level on the output changed which showed that the block was functional.

To test the second stage amplifier block, the light level was changed in the same way as above, and the output measured at the SMA output.

All the blocks were found to be working properly but unfortunately, signals from the transmitter block leaking to the receiver block were discovered. To avoid this all the devices were better decoupled with 470 nF capacitors presenting an impedance of 0.01 Ω at 12.5 MHz. This was calculated using the Murata chip S-parameter and impedance library computer program. Also a 1 μF capacitor was added for good measure.

These fixes removed most of the leaking signal, but not completely. To reduce coupling through the air, a metal shield was built using copper tape and cardboard, see picture 9.1. This reduced the noise from 12.3 mV to 6.96 mV at 12.5 MHz with a gain of 10 kΩ in the first stage and 30.8 in the second stage.

To eliminate the effect of the leaking signal, the LD driver and receiver circuits were finally completely separated by soldering them on two separate PCB:s. When these were mounted as described in section 9.2, the leakage signal was not observed again.

9.2 Measurement setup

In this section the measurement setup used for performing experiments on the system is presented.

9.2.1 Physical properties

The measurement setup which the authors consider to be the ideal setup is shown in figure 9.1. Here the transmitting and receiving circuits are separated onto two PCB:s, and the copper shield is mounted on the transmitting PCB. This ensures that the previously discussed leakage signal does not affect the measurements.

Furthermore, a black cardboard cone is placed such that it covers the edges of the lens on one end, and the area around the photodetector on the other. This keeps any laser light reflected from the lens holder from reaching the detector, while it helps blocking out ambient light when not measuring in darkness.

The two PCB:s were mounted in such a way that the spacing between the LD and the detector could be varied and tuned to the optimal spacing for each lens as discussed in chapter 3.

9.2.2 Reading values of the DSO

The target used for distance measurements was again a white A4 paper, but now with a small ring drawn in the center to help aiming. This target was moved manually for each new measurement point. The values of I and Q were read on the DSO screen and then imported into MATLAB for processing. Regarding the DSO settings when measuring the values of I and Q, a 1 MHz reference signal was used as trigger. Sampling was done over 128 values. The time resolution was kept at 5 ns, and the curves were zoomed in to a reliable level. Then the screen was paused, and the mean values were recorded. This setup was chosen specifically to mimic the behaviour of an ADC which may be used in a future system based on this receiver. Using the 1 MHz signal as a trigger and averaging over 128 measurement points implies a measurement speed of 1 MHz / 128 = 7.8 kHz which is close to the target speed in this project . A sampling rate of 1 Ms/s speed should be possible to achieve with a decent and not to expensive ADC. When measuring the actual signal level, the received signal was instead used as a trigger.

9.2.3 Targets

To investigate the effect of different target reflectivity, five papers were printed with varying percentage of printed ink. These were then in turn taped to the target located at a fixed distance from the detector, and a measurement was done for each paper. Furthermore, different types of textiles and other surfaces were placed at the target location, and more measurements were performed. Finally, using the white paper as target again, the effect of the angle of the target was measured, ranging from perpendicular to the incident laser beam to almost parallel with it.

9.2.4 Focusing and reference measurement

Focusing was done by holding a white piece of paper in front of the detector active area, and then adjusting the detector position using the turns on the optical bench until the focused laser dot appeared on its center. The distance at which this was done was far away enough to be considered infinity, but close enough to still see the dot with the naked eye. When measuring on short distances, the focused laser dot may miss the detector. In these cases the cone was removed and a refocus at this shorter distance was done.

The reference distance measurements were done using the UNI-T UT391 handheld distance meter with a specified accuracy of 1.5 mm.

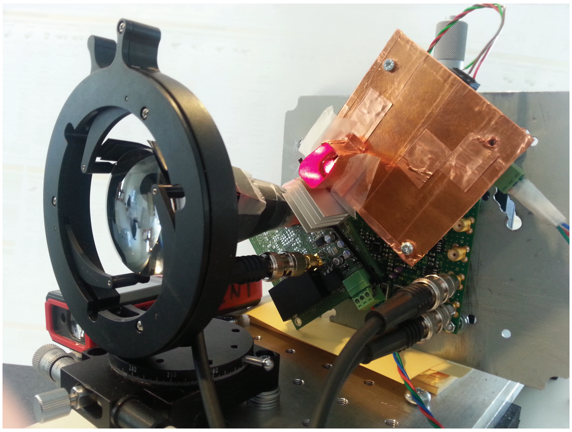

Figure 9.1: The ideal measurement setup.

9.3 Averaging

To investigate if the measurement precision is affected by averaging over different amounts of points, 15 distance measurements were done equidistantly between 1.48 m and 5.24 m using averaging over 4, 16, 64 and 128 points. As target a white A4 paper was used. The lens used had a diameter of 5 cm and a focal length of 10 cm. The focus was adjusted to be at optimum at about 3 m.

As described in section 9.2 there were some problems with measuring with the DSO. Furthermore, the setup used was not the optimum setup as described in section 9.2, since the LD driver circuit and the receiver circuit were still on the same PCB. Nevertheless, these measurements were carried out.

The values obtained in this measurement that obviously not corresponded to a distance were removed from the data set. A linear approximation was performed on the remaining data points, and the deviation from this approximation in each measurement point was plotted using MATLAB. This was done for all averaging conditions.

Chapter 10
Results

In this section the simulation as well as experimental results are presented, mainly in the form of MATLAB plots.

10.1 LD driver circuit

The results obtained in section 9.1.1 are presented in 10.1. It is clear that the driver circuit works as simulated. Figure 10.2 shows a transient analysis of the LD driver circuit which verifies the design. The measured result is shown in figure 10.3

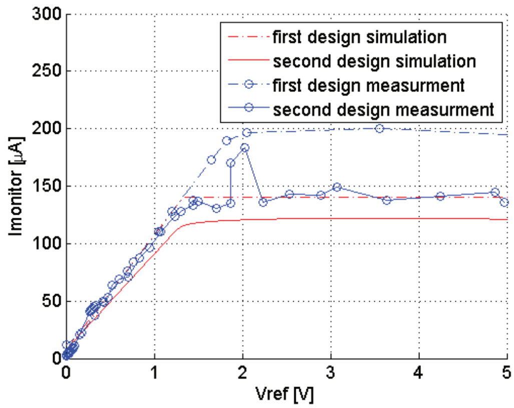

Figure 10.1: DC sweep for the LD driver circuit.

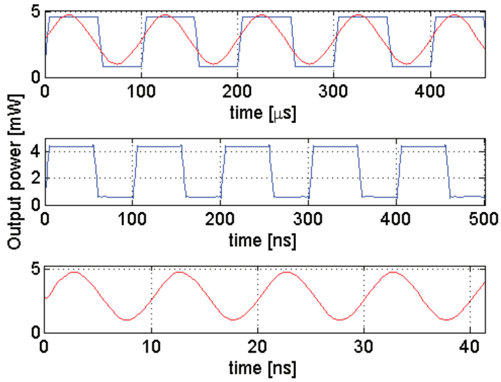

Figure 10.2: Transient simulations for laser driver circuit with 10 MHz square wave, 100 MHz sine wave and 10 kHz square and sine waves.

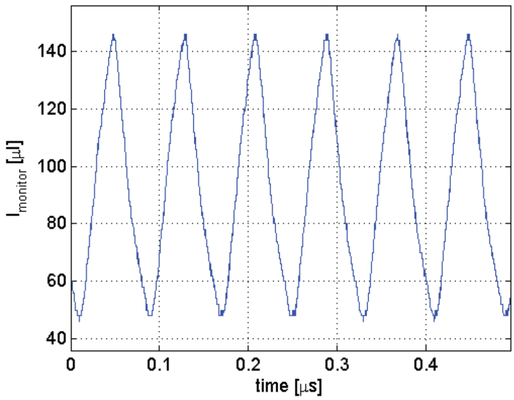

Figure 10.3: modulation measurement with 12.5 MHz triangle wave input.

10.2 Amplifier simulation

Here the results of the simulation of the amplifier stage gain are presented in figure 10.4.

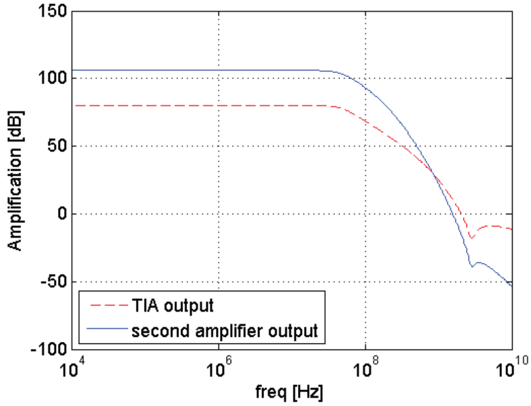

Figure 10.4: Gain of the amplifier when the TIA has 10 kΩ feedback resistor. The second stage has a gain of 20 dB.

10.3 Optimum setup

In figure 10.5 the measured vectors in the I-Q plane is shown. Each point represents a measurement value. In figure 10.6 the measured distance is shown together with the deviation from the linear approximation for each measurement value. It can be observed that the deviation is increasing with distance, except for the values for short distances. In figure 10.7 shows that the received signal power decreases with distance. Therefore it is logical to normalize the deviation by the square of the distance, which is done in figure 10.8. The standard deviation of this is calculated to be $\sigma/d^2 = 3.414610^{-4}$ m/m^2.

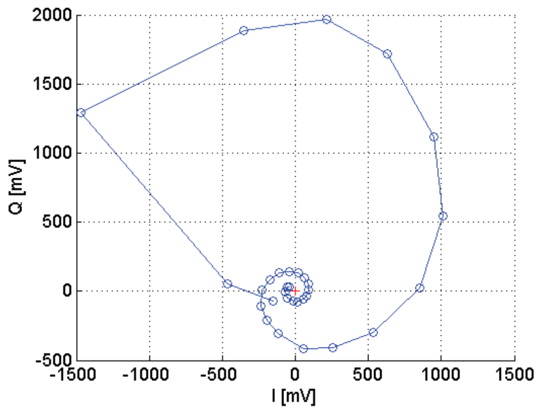

Figure 10.5: The IQ-phase plane.

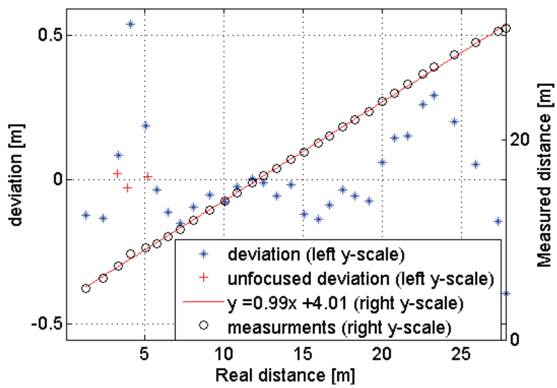

Figure 10.6: Measured distance versus real distance and deviation from the approximated line in each point. There is an offset in the measured distance which has not been compensated for. This is however a simple task left for future calibration.

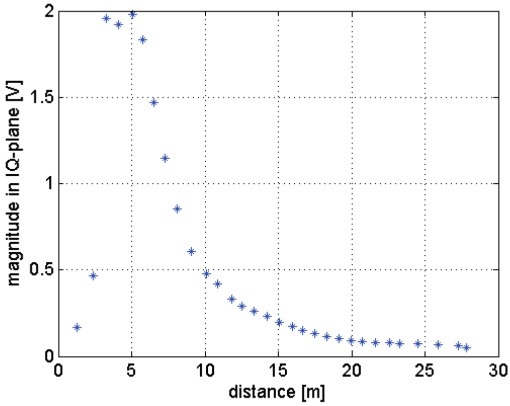

Figure 10.7: Magnitude in the IQ-phase plane.

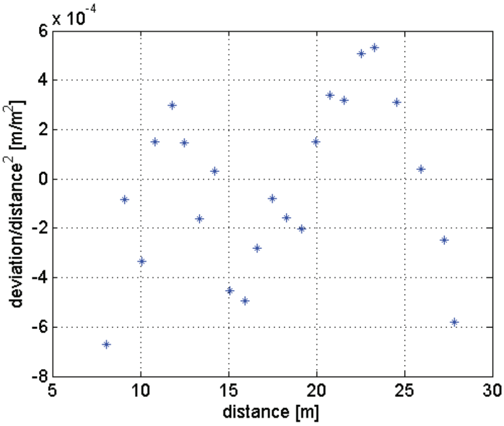

Figure 10.8: Deviation normalised on distance squared.

10.4 Detector

In this section the results from comparing the S10784 PIN diode and the S12023-10 APD are presented. The ideal measurement setup is used for both detectors. Figure 10.9 shows the normalized deviation. The APD to PIN ratio of the normalized standard deviation is calculated to be 4.86.

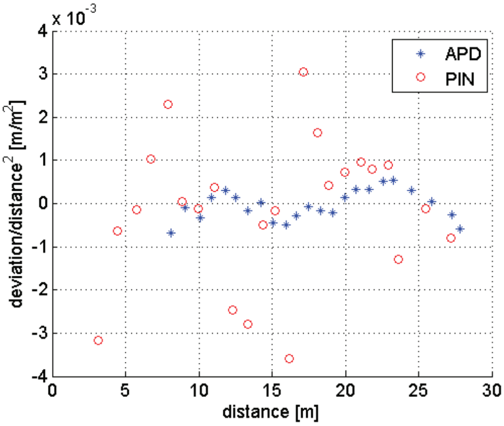

Figure 10.9: Deviation normalised on distance squared for PIN and APD diode.

10.5 Varying second stage amplifier gain

In this section two different gains of the second stage amplifier are compared. Figure 10.10 shows the normalized deviation for two gains corresponding to feedback resistors of 1.2 kΩ and 12 kΩ. The high to low gain ratio of the normalized standard deviation is calculated to be 0.48.

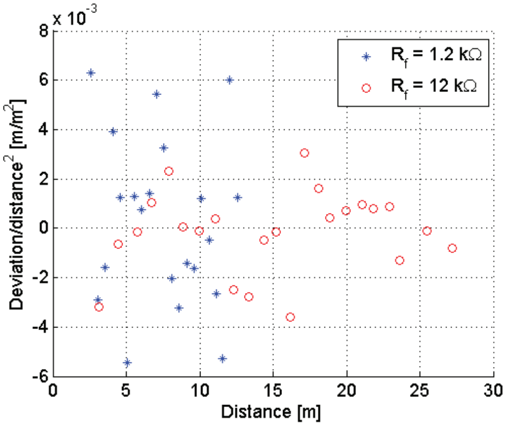

Figure 10.10: Deviation normalised on distance squared for different gains.

10.6 Ambient light level

In this section the result of the comparison between measurement in daylight conditions with lights on and dark conditions is presented. Figure 10.11 shows the normalized deviation for the two ambient light conditions. The light to dark ratio of the normalized standard deviation is calculated to be 0.49.

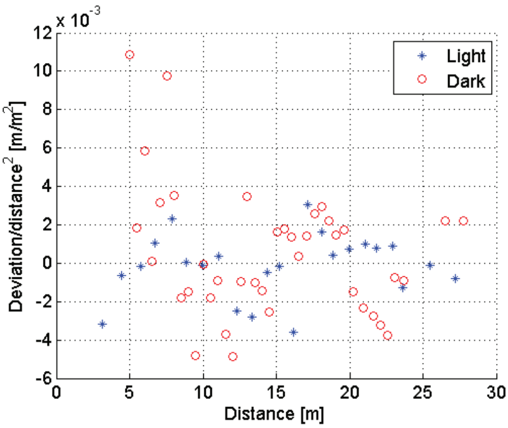

Figure 10.11: Deviation normalised on distance squared for different ambient light levels.

10.7 Target

In this section different target properties were investigated. The magnitude of the returned signal was measured for different targets and the results for some of the targets are shown in figures 10.12, 10.13 and 10.14.

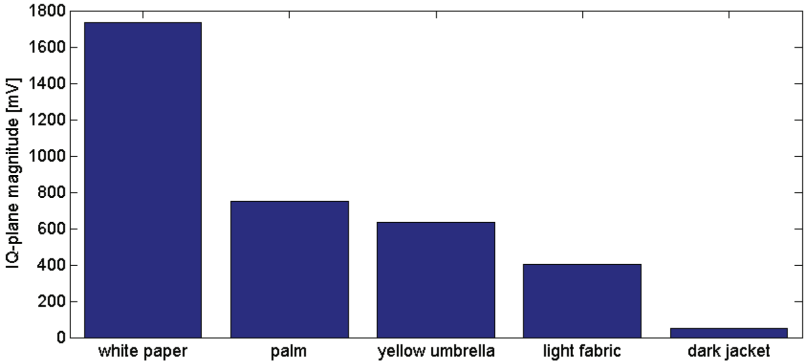

Figure 10.12: returned light for different target textures.

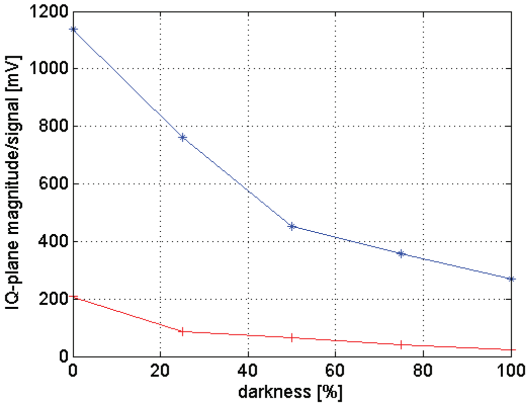

Figure 10.13: Returned light for different target darkness.

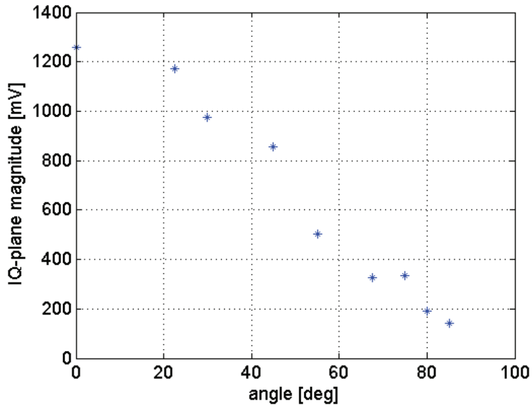

Figure 10.14: Returned light for different target angles.

10.8 Averaging

In this section the result from the averaging experiment is presented. Figure 10.15 shows the normalised deviation for different averaging settings. Figure 10.16 shows the calculated normalised standard deviation.

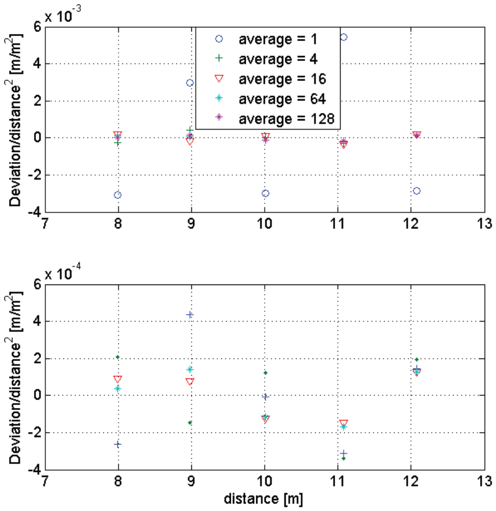

Figure 10.15: Normalised deviation for different levels of averaging.

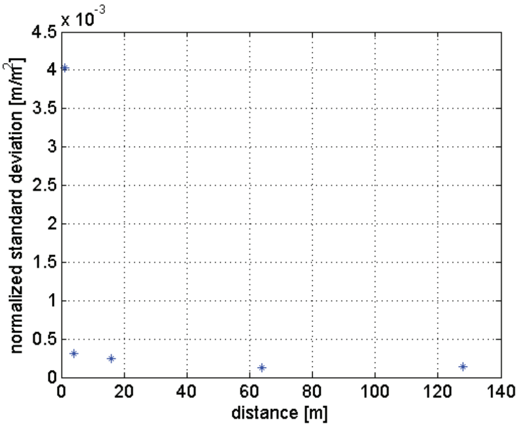

Figure 10.16: Normalised standard deviation for different levels of averaging.

10.9 Lens size

In table 10.1 the magnitude and normalised magnitude in the I-Q plane for different lenses is shown.

lens diameter [cm]	I-Q magnitude [V]	Normalised I-Q magnitude [V/m^2]
2.5	0.41	268
5	1.14	184

Table 10.1: Magnitude and normalised magnitude in the I-Q plane for different lens sizes

10.10 Calibration

From the results above it is seen that calibrating for a sinusoidal dependence might help in some cases. The result of the calibration is shown in figure 10.17 where the deviation is not calibrated and in figure 10.18 where it is calibrated. This gives a normalised standard deviation that is a factor 0.60 of the original.

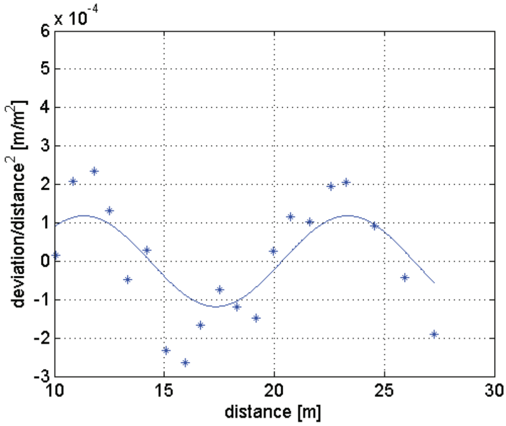

Figure 10.17: Uncalibrated normalised deviation.

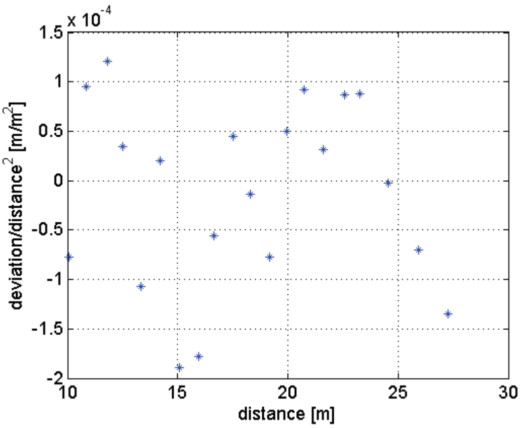

Figure 10.18: Calibrated normalised deviation.

Chapter 11
Discussion

In this chapter the results from the previous chapter are reviewed and discussed, and conclusions based on these are drawn. Future work suggestions are then given, both in the form of measurements on the existing setup that were not performed due to time constraints, and in the form of ideas for schemes which could be applied to improve performance.

11.1 Simulations

The LD driver circuit worked as simulated, since the measured data concurs well with the simulated data. The results from the amplifier gain simulation shows that the concept is feasible.

11.2 Measurments

The optimum setup was used in almost all measurements. Figure 10.5 shows the I-Q plane where each point corresponds to a measurement value. Here one can make a few observations. First, the largest magnitudes are obtained for the short distances while still being in focus. Secondly, as the distance increases, the magnitude of each vector decreases while the argument changes linearly, producing the spiral shaped curve.

From figure 10.6 one can see increased measurement uncertainty with increasing distance. It is interesting to note that the deviation seems to be periodic, which is seen even more clearly in figure 10.8, the reason for this is related to the values of the I and Q at certain points. When one of them is small in magnitude, the uncertainty increases due to the reduced SNR for that measurement. Secondly, a peak deviation is observed at 3 to 5 meters, and the reason for this was that in fact too much signal was obtained which saturated the receiving circuitry. This hypothesis was confirmed by repeating the measurement under intentional slight defocus, and this removed the peak.

Furthermore there is an offset in the measured distance curve in figure 10.6. This is caused by the time delay of the signal introduced by propagation through the receiver chain. The time delay is translated to a phase shift which directly gives a certain distance, and since the time delay and thus phase shift is constant the distance offset is also constant. It is a simple task to compensate for this offset, but even so, it is left for future calibration as it is not vital to the discussion in this project.

11.2.1 Varying second stage amplifier gain

The result shows that there is no accuracy improvement from using a higher second amplifier stage gain. However, the distance at which the signal could be detected was much larger in the case of higher gain. The reason for this behaviour may be that while the signal is amplified more with higher gain, so is the noise. Thus the SNR, and in turn the accuracy, will not improve by using more gain.

11.2.2 Detector

This result shows that the APD performs significantly better than the PIN diode. This may be due to the APD having internal gain, which increases the overall gain in the system. It may also be as in the case discussed above, that the system noise is dominated by thermal noise, and the APD would then provide higher SNR than the PIN diode.

Measurements on a PIN diode system with equal total gain are thus needed to truly verify this result. However, the previous gain experiment showed no accuracy improvement with increasing gain, and thus it is likely that the APD actually does perform better than the PIN diode. This comes at the cost of the increased complexity of the circuit involving large reverse bias as discussed above.

11.2.3 Ambient light level

The comparison between light and dark ambient light levels shows that higher accuracy is obtained during light conditions. By the previous noise discussion this seems highly unlikely, and taking into account all measurement error sources, a second measurement is needed to confirm this trend. Furthermore, these measurements were performed with a PIN diode, and the above results indicate that this diode has less accuracy than an APD, and thus repeating the measurement with an APD is expected to give a different result.

11.2.4 Target

The results show that different targets yield different amount of returned power. The distance which would be possible to measure under ideal conditions could thus not be measured for the less reflective materials. The returned power seems to be dependent on both target colour and texture as well as angle of laser beam incidence. Darker colour and textile targets reflected less light than lighter colour and smooth targets, as is intuitive. Less light is reflected back to the detector with increasing angle.

11.2.5 Averaging

The results from the average measurement show that averaging over more values yield better accuracy. The difference is largest between the measurement series where averaging was done over 4 values and the ones with more averaging. Not much difference is seen between the measurement series where more averaging was used, and this may be due to the fact that the measurements where done during 2.5 ns and averging over more time might help, further investigation into this is needed. Since averaging takes more time, the trade-off will be between measurement speed and accuracy if this is the case.

11.2.6 Lens size

The received power increases with larger lens area, but it does not increase directly proportional to the area which is shown in table 10.1. If that was the case, then normalizing with the area should cause the same value to be obtained for both lenses. This might be a result of measurement error since to the change lens, the setup had to be dismounted and then mounted again with the new lens. This implies a refocusing step which may affect the results significantly.

11.2.7 Calibration

Calibration helps in the case investigated, but further investigation is needed. It is not obvious where the sine dependency comes from but the hypothesis proposed in section 11.2 should be investigated further. If the mechanism responsible for this angular dependency is found it might be reduced and thereby removing the need for calibration altogether.

11.3 Conclusions

The most prominent result is the comparison between the PIN diode and APD receivers, which suggests that the APD is superior. Furthermore, target colour, texture and angle seems to affect the returned light power in an intuitive way, which would correspond to shorter maximum range with high accuracy for the system. The system measurement speed is estimated to be at least 8 kHz, which is considered fast compared to some existing laser range finders. The accuracy is however much lower, but some trade-off is expected between speed and accuracy.

11.4 Further work suggestions

Due to the interdisciplinary nature of this project, and the fact that it is a first investigation in the subject, there are many ways to continue this work. In this section the authors will on one hand list some interesting experiments on the existing setup that were not performed due to time constraints, and on the other hand introduce concepts that the authors find interesting for further development.

11.4.1 Schemes to increase output power

The 5 mW output power limitation is suitable for eye safe experimentation, but as discussed previously there are motivations for increasing the output power. During experiments one could allow for unsafe lasers if proper precautions are taken, but it would indeed be easier if the laser was safe. In a finished product eye safety is also very important, so the objective in this section is to maximize the output power subject to the constraint of keeping the laser eye safe.

Changing laser wavelength

The main motivation for wanting to emit higher power is to increase the range of the device. Considering again figure 5.2, it is clear that far-infrared light is not focused by the lens. Consulting the MPE tables for continuous emission of the wavelength 1550 nm and an accidental exposure of 10 s due to the corneal reflex not working in this regime, the value obtained is 10 mW. Already this is a factor 10 greater than for the wavelength of 650 nm used in this project.

Regular lenses for visible light can still be used at this wavelength, and there are photodetectors for this wavelength as well. [76] Though they tend to be less available and more expensive than the conventional detectors for visible light at large component distributors. This is because the bandgap of silicon is not suitable for detecting 1550 nm light, so instead some III-V material such as InGaAs must be used, which increases cost. Furthermore, LD:s in this region also seem more difficult to obtain compared to visible light lasers.

With an invisible beam it would also be harder to set up measurements and especially to obtain focus, so from a purely practical point of view a visible red laser at 650 nm is to be primarily used in this project.

A solution to the practical problems of using 1550 nm would be to install a visible laser diode to be used as aim. This would require precise alignment though, and was deemed to be beyond the scope of this project.

Pulsed operation

Inspired by commercial laser range finders (SICK DT50Hi) [16], another possibility would be to switch to pulsed operation. With sufficiently low duty cycle, i.e. short pulse length, a higher MPE per pulse than the MPE under CW operation should be possible to obtain. This is the case with the SICK DT50Hi, where the pulse power is 120 mW and the pulse length is 2.5 ns. The pulse repetition frequency (PRF) is 400 Hz, and all in all the laser is classified as class 1, i.e. safe for all viewing conditions. To investigate the possibilities of pulsed lasers for our application, the plot in figure 11.1 shows the MPE per pulse as a function of PRF, and the MATLAB code for the calculation is presented in appendix D.1.

The plot in figure 11.1 shows that shorter pulses gives higher output power. For a pulse length of 20 ns, due to pulses shorter than that being hard to achieve with the LD in this project, and a PRF of 100 kHz, the MPE per pulse is 490 mW. For a PRF of 1 MHz, the MPE per pulse has dropped to 49 mW, and at 50 MHz, one is essentially at the MPE for CW output. As discussed in section 2.1, the laser intensity modulation frequency decides what distances can be measured without ambiguities. Furthermore, from the discussion in section 2.1 it is clear that this frequency also affects the accuracy of the measurement since there is a lower bound for phase difference measurements set by the detector.

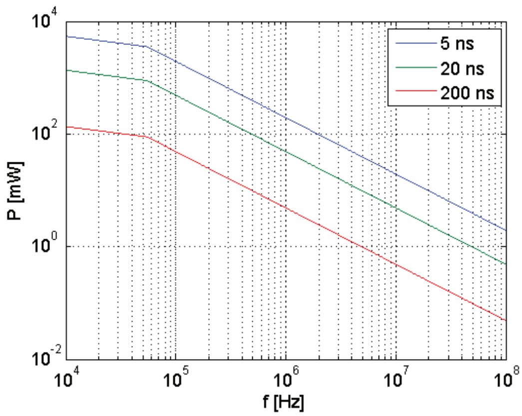

Figure 11.1: MPE as a function of PRF

The standard deviation in radians for 50 m, σ_{50} , is calculated using equation 11.1. Here $\sigma_{measured}$ is the normalised standard deviation measured with calibration, P is the signal power in the simulation and $P_{inmeasurement}$ is the measured signal power.

In the following simulations it is assumed that the usable power available in the measurements is 2.5 mW rather than the full 5 mW which is emitted due to severe losses in the suboptimal setup. For instance, the optical system is assumed to cause losses due to suboptimal focus and back reflection from the lens holder. The collimation of the laser beam is also far from optimal as the dot is approximately 15 cm in diameter at 27 m.

A simple approach to avoid ambiguities and allow for increased output power is to choose a frequency such that its period coincides with the maximum distance considered, and then reduce the duty cycle. For instance, if the maximum distance is 50 m, then a frequencies below 3 MHz provide adequate wrap around intervals of above 50 m. The standard deviation σ_d for these frequencies is calculated using equation 11.1. The corresponding standard deviation in meters is calculated using equation 11.2, where f is the frequency used for measuring. Figure 11.2 shows this standard deviation as a function of frequency, and as seen in this plot, the lowest standard deviation is 56 cm for frequencies above 55 kHz. However, the upper limit of 3 MHz still persist for ambiguity reasons. To reduce the standard deviation one needs to use higher frequencies, but a scheme to avoid ambiguities is needed.

$$\sigma_d = \frac{\sigma_{measured} d^2 \cdot P_{inmeasurment}}{P} \tag{11.1}$$

$$\sigma = \frac{\sigma_d \cdot c}{f \cdot 2\pi} \tag{11.2}$$

A scheme to allow higher frequencies and simultaneously increase accuracy is to use two frequencies, one low to determine the approximate distance, and one high to get the precision. A setup with dual lasers and detectors is possible for

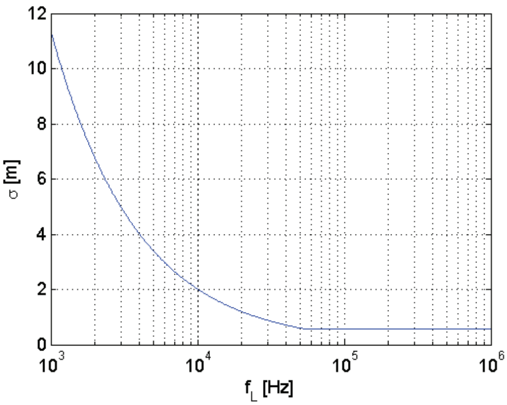

Figure 11.2: Standard deviation as a function of frequency for a maximum distance of 50 m.

this, but it is not very elegant. Thus, some kind of multiplexing would have to be applied to the beam in order to emit the two frequencies over the same signal. Pulsed operation may allow for a simple way of doing this, while simultaneously enabling higher MPE per pulse than the MPE for CW operation due to low duty cycle.

The idea is illustrated in figure 11.3. Essentially, the laser is modulated to emit pulses with low frequency, f_L, to measure an approximate distance, this is then the PRF. The low PRF and relatively short pulses allows for high MPE. Each pulse is then modulated with the higher frequency, f_H to measure more accurately. The ambiguity is removed using the information provided by the lower frequency. The PRF has to be high enough to be able to decide which interval of the higher frequency signal period the distance corresponds to, see equation 11.3, where σ_d is in radians, and it is calculated using equation 11.1. The factor 2 represents that the measured value is within 2 standard deviations, i.e. to get a correct measurement in 95 % of the cases. To be able to measure the signal with f_H each pulse of the f_L should contain a minimum number of periods and have a minimum length.

$$f_H > \frac{F_L \cdot 2\pi}{2\sigma_d} \tag{11.3}$$

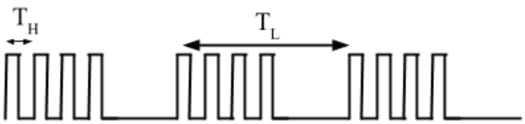

Figure 11.3: Concept for pulse modulation. The period of f_L and f_H is shown.

To test the concept it is assumed that 5 pulses is sufficient to be able to measure the phase difference and a minimum pulse length of 100 ns is considered minimum. The script works in the following way. f_L is swept from 3 kHz to 3 MHz and P is swept between 1 and 0 W. Formula 11.1 is used to calculate the maximum standard deviation and this in turn is used to calculate f_H with equality assumed in equation 11.3. The script then checks if this complies to the laser safety rules for a class 2 laser, i.e. safe under accidental exposure of 0.25 s as discussed in chapter 5.1. The standard deviation in meters is then calculated with equation 11.2 and the smallest value still complying to the laser regulations is ploted versus f_L. The script is found in appendix D.2.

It is clear that for f_L higher than 52 kHz satisfies the desired distance condition of 50 m while still being eye safe. The lowest standard deviation, 2.9 mm, is found at 52 kHz. So with this scheme a considerably lower standard deviation is achieved than with only one frequency.

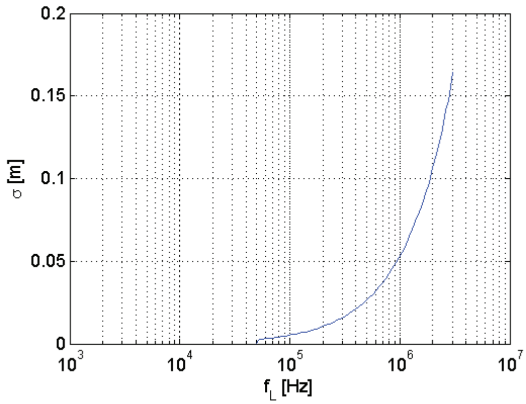

Figure 11.4: standard deviation as a function of f_L as investigated as a future work scheme to increase Laser output power while remaining eye safe.

A more problematic matter, at least in this project, of this scheme is to actually generate the signal shown in figure 11.3. It would probably be easiest to generate it digitally and then use digital to analog converters, but this is beyond the scope of this project. Furthermore, with the current setup involving the AD8333 I-Q demodulator IC, there would be additional requirements on the signal generation, such as the fact that four times the frequency must be generated simultaneously with correct phase. Even then one could only make the distance measurement with one frequency only, as the two channels in the demodulator shares the LO signal.

Regarding the additional receiver architecture requirements, the signal would have to be split after sufficient amplification, and then the f_L signal might have to be passed through a low pass filter to get a 50 % duty cycle. This may be necessary to ensure that the mixer can operate properly. The DC output level of the two I-Q mixers for each step would then be used to calculate the distance based on the two different frequencies, and the ambiguity of the high frequency signal removed using the low frequency signal information using some simple program.

11.4.2 Measurements

First of all, measurements using all of the purchased photodetectors instead of just some of them could be done. These could confirm the trends observed with the used photodetectors, and possibly be used to draw more conclusions about the performance of each type of detector. Furthermore, some of the measurements performed should perhaps be redone, following the discussion regarding the initial uncertainty of the DSO measurements.

Throughout this report it is assumed that the phase accuracy of the detector is independent of frequency. A simple test for this is to simply switch the crystal oscillator to one with another frequency and perform a new measurement series. Comparing then deviation from the approximated in the two crystal oscillator cases should at least give an indication as to wether or not the assumption is valid.

Another assumption is that higher LD output power leads essentially leads to better range performance by increasing the SNR. This theory could either be investigated by using a high output power LD and verifying it directly, or by reducing the intensity of the emitted laser light by using ND filters. If the SNR decreases in this case, then lower output power means worse range performance, and the opposite should therefore be true.

The cascode front-end should be investigated as well. The design offers the possibility to simply add this part to the system. For future applications it is expected to be particularly interesting for the PIN diode receiver circuit, since it is such a cheap device and requires so little practical considerations compared to an APD. It would be interesting to know how much, or if at all, better the circuit could become.

The effect of the optical bandpass filter should be more closely investigated. In this project all that has been done in this direction is to conclude that it rather effectively removes background noise in the form of ambient light, but that it has quite low transmission even at the pass band. Also, there are indications that the alignment is important.

Finally, the low pass filter present on the output of the IQ-demodulator evaluation board has been kept constant at 90 kHz. From the ADS simulations it is expected that the speed of this filter sets the speed of the receiver system. It would be interesting to compare e.g. the measurement accuracy for different low pass filter speeds. This could be useful information when considering implementation, as depending on the situation, one may wish to optimize for either measurement accuracy or speed.

Chapter 12
Summary

The design presented in this thesis is based on a review of different system architectures as well as a theoretical analysis of available photodetectors. Different circuit topologies have been simulated in LTSPICE to determine suitable schematics and component values. Two PCB layouts has been produced and realised. Both systems have been experimentally evaluated.

The result is the design and realisation of a complete laser range finding system which has been shown to measure distances of up to 27 m with a maximum deviation of 30 cm. The measurement speed is estimated to at least 8 kHz. The system has been designed using ordinary components which are available off-the-shelf with large component distributors.

Comparing this result with the goals stated in the beginning of the thesis, it is not very far away, and there is much potential for improvement. Thus the result is considered satisfactory as a first investigation in the subject and as a proof of concept. With more time and just minor tweaks, the authors are certain that a better system could be designed. The future work suggestions presented are those which the authors believe are the most worth wile pursuits for improving performance.

References

[1] Laser Distance-Measuring Techniques Annual Review of Earth and Planetary Sciences Vol. 5: 357-369 (Volume publication date May 1977)

[2] Meaghan Weir, *Tigers prepare: Remain on radar*, [Online], `http://tigersprepare.blogspot.se/2011/09/remain-on-radar.html` [2014-06-10]

[3] Dr. Rüdiger Paschotta, *Distance Measurements with Lasers*, [Online], `http://www.rp-photonics.com/distance\_measurements\_with\_lasers.html` [2014-05-27]

[4] Harnesk Carina, *Heimdall laser rangefinder*, [Online], `http://www.saabgroup.com/en/Land/Weapon-Systems/Laser\_Rangefinder/HEIMDALL\_Laser\_Rangefinder/` [2014-05-28]

[5] PCE Instruments UK Ltd, *Laser distance meter DLS-CH15*, [Online], `http://www.pce-instruments.com/english/measuring-instruments/installation-tester/laser-distance-meter-dimetix-ag-laser-distance-meter-dls-ch15-det\_61472.htm?\_list=kat\&\_listpos=20` [2014-05-28]

[6] RobotShop Distribution inc, *Hokuyo UTM-30LX Scanning Laser Rangefinder*, [Online], `http://www.robotshop.com/en/hokuyo-utm-03lx-laser-scanning-rangefinder.html\#Specifications` [2014-05-28]

[7] FLT Geosystems & LSR, *Demo Leica ScanStation C10 Laser Scanner (hardware only) (EA)*, [Online], `http://www.fltgeosystems.com/used-surveying-equipment/demo-leica-scanstation-c10-laser-scanner-hardware-only-demo-leica-scanstation-c10/` [2014-05-28]

[8] PCE Instruments UK Ltd, *Laser Distance Meter Prexiso iC4*, [Online], `http://www.pce-instruments.com/english/measuring-instruments/installation-tester/laser-distance-meter-laser-distance-meter-prexiso-ic4-det\_407130.htm?\_list=kat\&\_listpos=1` [2014-05-28]

[9] RobotShop Distribution inc, *Parallax 15-122cm Laser Rangefinder*, [Online], `http://www.robotshop.com/en/parallax-15-122cm-laser-rangefinder.html` [2014-05-28]

[10] Brian Benchoff, 2014, *Homebrew Phase Laser Rangefinder*, [Online], http://hackaday.com/2014/02/28/homebrew-phase-laser-rangefinder/ [2014-05-28]

[11] Laserdeveloper, 2013, *Designing a Laser Range Finder*, http://forums.hackaday.com/viewtopic.php?f=3\&t=3490 [2014-05-28]

[12] SparkFun Electronics, 2012, *Project/product: high res/update rate laser rangefinder*, [Online], https://forum.sparkfun.com/viewtopic.php?f=14\&t=33052 [2014-05-28]

[13] Geoffrey L. Barrows, 2012, *11 gram Arduino-powered laser rangefinder*, [Online], http://diydrones.com/profiles/blogs/11-gram-arduino-powered-laser-rangefinder [2014-05-28]

[14] Peter McInnes PTY LTD, *Neato's Features*, [Online],http://www.neatorobotics.com.au/how-it-works/features\#laser_mapping [2014-05-28]

[15] Leica Geosystems AG, 2010, *Leica HDS6200*, [Online], http://www.oceanscan.net/gallery/PDFs/Leica\%20HDS6200\%20DAT_en.pdf [2014-05-28]

[16] SICK AG, *Mid range distance sensors*, [Online], https://www.mysick.com/ecat.aspx?go=FinderSearch&Cat=Row&At=Fa&Cult=English&FamilyID=402&Category=Produktfinder&Selections=53613 [2014-05-28]

[17] PCE Instruments UK Ltd, *Laser Distance Meter PCE-LDM 50*, [Online], http://www.pce-instruments.com/english/measuring-instruments/installation-tester/laser-distance-meter-pce-instruments-laser-distance-meter-pce-ldm-50-det_61084.htm?_list=kat\&_listpos=2 [2014-05-28]

[18] Chris Anderson, 2009, *$30 laser rangefinder!*, [Online], http://diydrones.com/profiles/blogs/30-laser-rangefinder [2014-05-28]

[19] Palojärvi Pasi, 2003, *Integrated electronic and optoelectronic circuits and devices for pulsed time-of-flight laser range finder*, Ph.D. Thesis, University of Oulu, availible: http://herkules.oulu.fi/isbn9514269667/isbn9514269667.pdf [2014-02-14]

[20] a cam-me s sele ct roni c gmbh, 2013, *Application Note 034: Laser Range Finder with the TDC-GP22*, http://www.pmt-fl.com/downloads/tdc/AN034_en.pdf [2014-03-22]

[21] Dr. Rüdiger Paschotta, *Optical Heterodyne Detection*, *Optical Heterodyne Detection*, http://www.rp-photonics.com/optical_heterodyne_detection.html [2014-03-22]

[22] Adany, Peter, 2007, *Simplified Homodyne Detection for FM Chirped Lidar*, M.Sc. Thesis, available: http://hdl.handle.net/1808/1982 [2014-05-29]

[23] Collimation Tutorial, 2014, *Thorlabs Tutorials*, http://www.thorlabs.com/tutorials.cfm?tabID=38696 [2014-06-16]

[24] Laser Institute of America, 2007, *ANSI Z136.1. American National Standard for Safe Use of Lasers*, Orlando: LIA

[25] Rockwell Laser Industries, Inc., *Laser Standards and Classifications*, http://www.rli.com/resources/articles/classification.aspx [2014-05-22]

[26] Office of Radiation Safety University of Chicago, *Calculating MPE and NHZ*, http://safety.uchicago.edu/files/Laser\%20MPE\%20and\%20NHZ\%20Calculations.pdf [2014-05-22]

[27] Ming Lei, Hong Li, Zhiyong Lei, Xing Liu, 2011, Research on Detection Performance in Laser Ranging System, *2011 International Conference on Computer Science and Information Technology*, Singapore, 31 march 2011

[28] Nick Bertone, Paul Webb, *Noise and Stability in PIN Detectors*, http://bellota.ele.uva.es/~pedro/optoele/photodiodes/noise.pdf [2014-05-19]

[29] *Noise-equivalent power*, https://www.princeton.edu/~achaney/tmve/wiki100k/docs/Noise-equivalent_power.html [2014-05-19]

[30] Boulder, 2004, *Principles of Semiconductor Devices*, http://ecee.colorado.edu/~bart/book/book/chapter4/ch4_2.htm [2014-05-29]

[31] S.M. Sze. Semiconductor Devices Physics and technology. 2nd ed. Wiley. 2002.

[32] Dr. Rüdiger Paschotta, *Photodiodes*, http://www.rp-photonics.com/photodiodes.html [2014-05-21]

[33] Bahaa E. A. Saleh, Malvin Carl Teich. Fundamentals of Photonics. John Wiley & Sons, Inc. 1991.

[34] Resistor Guide, *Photo resistor*, http://www.resistorguide.com/photoresistor/ [2014-05-18]

[35] PerkinElmer Optoelectronics, *Photoconductive Cell VT900 Series*, http://www.farnell.com/datasheets/919043.pdf [2014-05-19]

[36] Burle Industries Inc, *Photomultiplier Handbook*, http://psec.uchicago.edu/links/Photomultiplier_Handbook.pdf [2014-05-19]

[37] Ian Poole, *Phototransistor Tutorial*, http://www.radio-electronics.com/info/data/semicond/phototransistor/photo_transistor.php [2014-05-19]

[38] Chris McFee, *An introduction to CCD operation*, http://www.mssl.ucl.ac.uk/www_detector/ccdgroup/optheory/ccdoperation.html [2014-05-20]

[39] Umezawau Toshimasa1 Kudou Takahiro1 Hihara Mamoru2 Wada Morio, 2008, *Dual PIN Photodiode For Phase Shift Keying Optical Telecommunication Systems*, http://cdn2.us.yokogawa.com/rd-tr-r00046-006.pdf [2014-05-29]

[40] Edmund Optics Inc., *Hamamatsu Photomultiplier Tube Modules*, http://www.edmundoptics.com/electro-optics/detector-modules/hamamatsu-photomultiplier-tube-modules/2512 [2014-05-20]

[41] Vishay Semiconductors, 2013, *Silicon PIN Photodiode VEMD10940F* http://www.vishay.com/docs/84171/vemd10940f.pdf [2014-05-20]

[42] First Sensor AG, 2012, *First Sensor APD Data Sheet Part Description AD1500-10 TO*, http://se.mouser.com/ProductDetail/First-Sensor/AD1500-10-TO5I/?qs=sGAEpiMZZMs50KUSuyRkpu5Ln7emvXOLmfog4MOtzrg%3d [2014-05-20]

[43] Princeton University, Cross section of the human eye, [image online], http://web.princeton.edu/sites/ehs/laserguide/sec2.htm [2014-05-22]

[44] Arima Lasers, *AlGaInP Visible laser diode ADL65075TL*, https://www1.elfa.se/data1/wwwroot/assets/datasheets/adl65075tl_eng_tds.pdf [2014-06-02]

[45] Fiber-Optics, *Laser Diodes*, http://www.fiber-optics.info/articles/laser_diodes [2014-06-02]

[46] Laser Components, *AlGaInP Visible laser diode ADL65055TL*, https://www1.elfa.se/data1/wwwroot/assets/datasheets/cv632502.pdf [2014-06-02]

[47] Analog Devices, Inc., *AD8021*, https://www1.elfa.se/data1/wwwroot/assets/datasheets/nrAD8021_e.pdf [2014-06-02]

[48] Philip C. D. Hobbs, 2001, *Photodiode Front Ends The REAL Story*, http://www.electrooptical.net/www/frontends/frontends.pdf [2014-05-28]

[49] David R. Kirkby, 1999, *A Picosecond Optoelectronic Cross Correlator using a Gain Modulated Avalanche Photodiode for Measuring the Impulse Response of Tissue*, Ph.D. Thesis, http://www.medphys.ucl.ac.uk/research/borl/docs/dkirkby.pdf [2014-05-28]

[50] Walter R. Leeb,1989, *Degradation of signal to noise ratio in optical free space data links due to background illumination* Optical Society of America

[51] S. Blair, 2012, *Notes from the course ece5411*, http://www.ece.utah.edu/~blair/T/ece5411/notes/3_28_12.pdf [2014-06-16]

[52] Philip C. D. Hobbs. BUILDING ELECTROOPTICAL SYSTEMS. Wiley. 2009

[53] Philips Semiconductors, 1997, *BFR93 NPN 5 GHz wideband transistor*, https://www1.elfa.se/data1/wwwroot/assets/datasheets/fj611025_e.pdf [2014-06-02]

[54] Brian Hirasuna, 2000, *Modeling Photodiodes, LEDs and Laser Diodes*, http://www.orcad.com/documents/community.an/pspice/tn27.aspx [2014-03-02]

[55] D.J.A. Groeneveld, 2010, *Bandwidth extension and noise cancelling for TIAs*, http://essay.utwente.nl/59736/1/MA_thesis_D_Groeneveld.pdf [2014-06-10]

[56] Texas Instruments Inc., 2008, *OPA847 Wideband, Ultra-Low Noise, Voltage-Feedback OPERATIONAL AMPLIFIER with Shutdown*http://www.ti.com/lit/ds/symlink/opa847.pdf [2014-03-02]

[57] Jeff Falin, Texas Instruments Inc., 2003, *Reverse Current/Battery Protection Circuits*http://www.ti.com/lit/an/slva139/slva139.pdf [2014-06-16]

[58] David Westerman, 2007,*Understand and apply the transimpedance amplifier*, http://www.planetanalog.com/document.asp?doc_id=527534

[59] Dipak Basu, 2000, *Dictonary of pure and applied physics*, Boca Raton: CRC Press LLC

[60] *TIA Bode Plot 0S*, http://en.wikipedia.org/wiki/Transimpedance_amplifier#mediaviewer/File:TIA_Bode_Plot_0S.svg [2014-06-10]

[61] Analog Devices, Inc, *ADA4939-1/ADA4939-2*, http://www.analog.com/static/imported-files/data_sheets/ADA4939-1_4939-2.pdf [2014-03-02]

[62] Analog Devices, Inc., *AD8343*, http://www.analog.com/static/imported-files/data_sheets/AD8343.pdf [2014-03-02]

[63] Linear Technology Corporation, *LTC6906*, http://cds.linear.com/docs/en/datasheet/6906fc.pdf, [2014-03-02]

[64] ECS inc., *ECS-3961/3963 SMD CLOCK OSCILLATOR*, http://www.ecsxtal.com/store/pdf/ecs-3961_3963.pdf, [2014-06-02]

[65] ECS inc., *ECS-3951M/3953M-BN SMD CLOCK OSCILLATOR* , urlhttp://www.ecsxtal.com/store/pdf/ecs-3951m-bn-3953m-bn.pdf [2014-06-02]

[66] RECOM Electronic GmbH., 2014, *INNOLINE DC/DC-Converter*, http://www.recom-international.com/pdf/Innoline/Rxx-B.pdf [2014-06-02]

[67] EEWeb, *Microstrip Impedance Calculator*, http://www.eeweb.com/toolbox/microstrip-impedance [2014-06-02]

[68] Analog Devices, Inc., *AD8333 DC to 50 MHz, Dual I/Q Demodulator and Phase Shifter*http://www.analog.com/static/imported-files/data_sheets/AD8333.pdf [2014-06-02]

[69] Analog Devices, Inc., *ADA4817-1/ADA4817-2 Low Noise, 1 GHz FastFET Op Amps*http://www.analog.com/static/imported-files/data_sheets/ADA4817-1_4817-2.pdf [2014-06-02]

[70] Fairchild Semiconductor Corporation, 1993, *74VHC4040 12-Stage Binary Counter*, http://www.fairchildsemi.com/ds/74/74VHC4040.pdf [2014-06-02]

[71] Analog Devices, Inc., *ADM7150 800 mA Ultralow Noise, High PSRR, RF Linear Regulator*, http://www.analog.com/static/imported-files/data_sheets/ADM7150.pdf [2014-06-02]

[72] Texas Instruments Inc., 2013, *LM2990 Negative Low Dropout Regulator*, http://www.ti.com.cn/cn/lit/ds/symlink/lm2990.pdf [2014-06-02]

[73] Silicon Sensor International AG, *Silicon Sensor APD Data Sheet Part Description AD100-12 SMD*, http://www.pacific-sensor.com/pdf_s12/AD100-12-LCC6.1fprelim.pdf [2014-05-29]

[74] Hamamatsu photonics K.K., *S12023 series, etc.*, https://www.hamamatsu.com/resources/pdf/ssd/s12023-02_etc_kapd1007e12.pdf [2014-05-29]

[75] Excelitas Technologies Corp., *C30902 and C30921 Series High-speed solid state detectors for low light level applications*, http://www.excelitas.com/downloads/DTS_C30902_C30921.pdf [2014-05-29]

[76] California Estern Labratories, 2003 *PHOTO DIODE NR8300FP-CC*, http://www.cel.com/pdf/datasheets/nr8300fp.pdf [2014-05-23]

Appendices

Appendix A

First design

In this appendix the design and evaluation results of the first design is presented. This analysis has been placed in this appendix as to not interfere with the discussion of the second design which is considered the main design of the project and on which all the discussion in the main report is based on.

A.1 Transmitter circuit design

The transmitter circuit is almost identical for the two designs. The only difference is that for the first design a ±12 V supply is used instead of a ±5 V supply. The associated circuit differences are so minor that the schematic for the first design is omitted.

A.2 Receiver circuit design

The schematic of the receiver circuit for the first design is also very similar to the one used for the second design. As transimpedance amplifier the OPA847 was used, while the fully differential ADA4939 [61] was used as the second stage amplifier in the configuration shown in figure A.1. Here the gain for the single-ended to differential conversion is given by $G \approx R_f \ / \ R_g$. A fully differential op amp was chosen since the mixers used had differential input, and a stage to convert from single-ended signal to differential signal was anyway needed. Only two gain stages were employed since active mixers were chosen.

A.3 Second stage

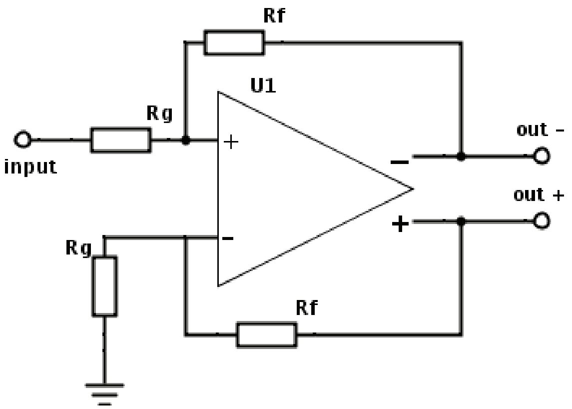

Figure A.1: Schematic for the fully differential second stage amplifier.

A.4 Signal generation

To be able to investigate the effect of using different frequencies and wave forms, three signal generators for square and sine waves are designed; one which is tunable between 10 kHz and 1 MHz, and two that are fixed at 10 MHz and 100 MHz respectively. The schematic used for all three signal generators is shown in figure A.2.

The tunable signal generator is the LTC6906 circuit from Linear Technology [63], which generates a square wave whose frequency is tuned by a resistor not shown in the schematic. The remaining two generators use crystal oscillators [64] [65] to generate square waves at their fixed frequencies. $C1$ removes the DC part of the oscillator output signal and $R1$, $L1$ and $C2$ works as a simple second order low pass filter. This attenuates the harmonics from the square wave which results in a decent sine wave. $R1$ is simply soldered off when a square wave is needed.

These circuits were modelled and simulated in LTSPICE to verify their correct operation as well as for fine tuning component values. These results are omitted to keep focus on other, more important results.

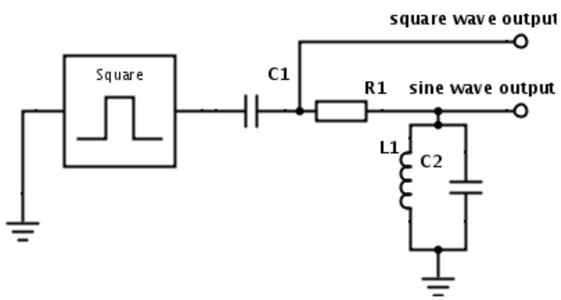

Figure A.2: schematic for signal generation.

A.5 Mixers

As mentioned above, the next stage in the receiver chain is the mixer stage. The mixer has to have sufficient bandwidth and be able to do direct conversion down to baseband, which in this case is DC. The part $AD8343$ from Analog Devices [62], which is an active 2.5 GHz mixer, was chosen because it fullfils the demands and provides additional gain.

A.5.1 Simulation

LTSPICE simulation of the mixer stage could not be performed because no model was available for them. Ideal mixer models were used in the system simulation described in section 7.4.

A.6 Phase shifter

The quadrature receiver architecture is based on mixing the returning signal with a 90° phase shifted local oscillator signal. To perform this phase shift, an active all-pass filter may be used as phase shifting circuit. The schematic of such a phase shifter is shown in figure A.3. Here, $R3$ and $C1$ constitutes a high pass filter with corner frequency

$$f_c = \frac{1}{2\pi R_3 C_1}, \tag{A.1}$$

providing the phase shift of 90° at the desired frequency. The gain is set by $G = R1 \ / \ R2$, and by putting $R1 = R2$ the attenuation introduced by this high pass filter is removed. For higher frequencies than the desired one, C_1 looks like a short and the circuit behaves like a non-inverting unity gain amplifier without phase shifting the signal. For lower frequencies C_1 instead looks open, and the circuit will instead behave like an inverting unity gain amplifier, thus causing a 180° phase shift.

As an example, if the frequency of interest is 1 MHz, then suitable component values are $C_1 = 15.9$ pF and $R_1 = 10$ kΩ, which gives $f_c = 1.0$ MHz. To maintain unity gain, $R_1 = R_2 = 100\ \Omega$ may be chosen. The circuit was simulated in LT-SPICE with these component values and those corresponding to other frequencies, and adequate behaviour was observed in all cases. These results are omitted as they are not vital to further discussions.

A.6.1 Power supply

When connecting the first design board to the power supply, it so happened that a couple of times the polarities where accidentally reversed. The result in each of these accidents was that many of the components were destroyed and had to be replaced, which was expensive and rather time consuming. No reverse polarity protection was implemented in the first design.

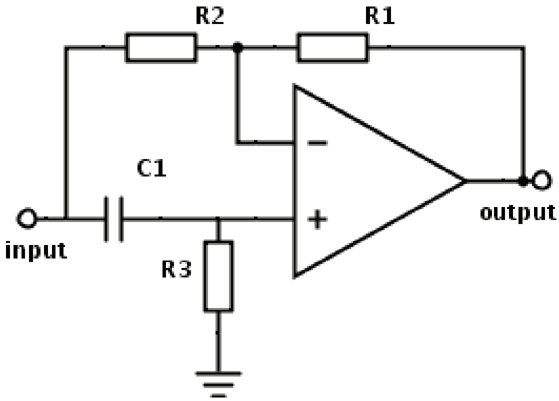

Figure A.3: Schematic for the phase shifter.

A.6.2 Output low pass filter

On the mixer outputs the ability to add a low pass filter was implemented. This was intended to enable experimentation on the system measurement speed and accuracy. Unfortunately, due to the many non-working stages in the design, this stage was never evaluated.

A.7 PCB layout

In figure A.4 it is important to note that since there were 5 photodiode locations but only one laser diode location, the distance between the detectors and the LD was very long. This is because when the PCB layout was done, the analysis in section 3.2.1 had not yet been done. Hence none of the conclusions regarding the relative placing of the LD and PD could benefited from. In essence, the same steps during the PCB layout were taken for both designs, and these are stated in the main report.

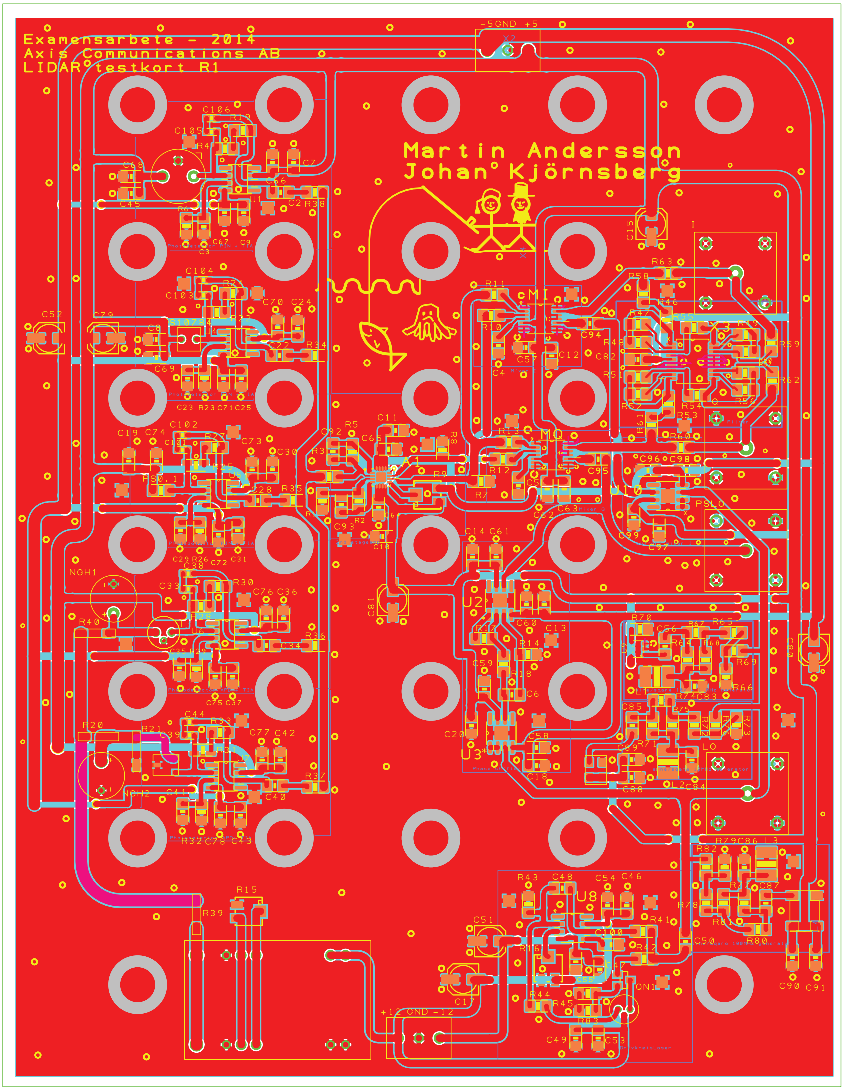

Figure A.4: PCB layout. The large grey coloured vias were added to facilitate PCB mounting on the measurement setup.

A.8 Evaluation

To test the second stage amplifier block, the light level was changed at the photodetector, and the a probe was used to measure the output signal. Despite several attempts and change of configuration, this stage was never found to function correctly. The authors suspect that the main issue was that the device footprint was such that it was very hard to solder correctly. In the end, the amplifier had to be bypassed with a cord.

The phase shifter was tested by feeding the signal from the signal generator to both the oscilloscope and the phase shifter and the measure the output from the phase shifter simultaneously. The phase shift was then measured with cursors in the oscilloscope. The phase shift was as close to $90°$ as the oscilloscope could measure.

The mixers were tested by sending the laser beam back to the photodiode with a mirror, and thereby achieving a phase difference between this signal and the local oscillator. This was mixed with the LO signal and the output was measured. This test did not generate the desired output since the mixer required external biasing on the output. To achieve conversion to DC was therefore hard, if not impossible.

The output from the signal generators was measured both when square and sine waves were produced. These were found to function correctly in all cases.

A.9 Measurements

Only a few measurements were performed on the first design, as its performance was truly unsatisfactory. It however served as an indication that the concept worked. As mentioned above, correct mixer operation was not obtained, and as such the evaluation board used extensively with the second design was used during the measurements with the first design as well.

A.9.1 Returned light distance relationship

To investigate the intensity of the returned light as a function of distance to the object, the signal from the S10784 and TIA was amplified further by connecting, via cord, a second OPA847 in the inverting configuration with a gain of 12 dB in order to get a measurable signal. The LD output power was modulated with a 12.5 MHz signal between 0 and 5 mW. The laser beam was directed at a white paper (A4) at a distance that was varied during the experiment. The board position relative to the lens was adjusted to achieve optimum focus on the PD for that distance. These adjustments were necessary due to the PD being placed too far away from the LD on the first design board.

The signal level peak to peak was measured for 6 different distances between 0.5 m and 2 m. This was converted to received power by dividing the measured signal level by the gain in the circuit. To identify the relationship between distance and received power the logarithm was taken and a linear approximation was made, see figure A.5. The relationship is then calculated to $P_{recived} = 2.42 \cdot 10^{-7}/d^{1.75}$, see figure A.6.

A.9.2 Distance measurement with the IQ-demodulator

The measurement setup in section A.9.1 was used in this case as well. The strategy described in chapter 7.3 for generation of the RF and LO signals was employed in the first design as well. However, as there was no footprint for the binary counter on the first design board, creative modifications of the board had to be done. The board was then connected to the IQ-demodulator evaluation board via BNC cables.

The I and Q were measured at 10 cm intervals between 0.5 and 1.5 m, see figure A.7. The estimated distance was calculated using equation 2.2.

A.10 Results

In this section the results of the measurements with the first design board are presented.

A.10.1 Returned light distance relationship

The results in figures A.5 and A.6 can be compared to equation 3.1 where the expected relationship was dependence on the inverse square of the distance.

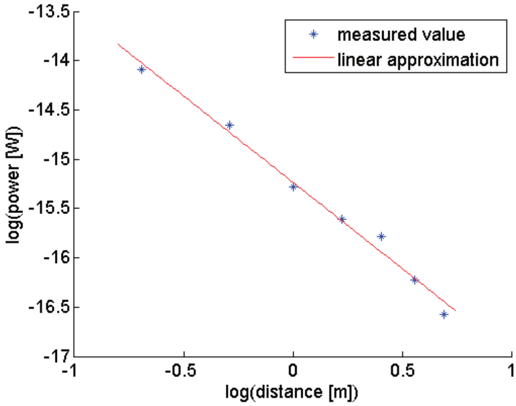

Figure A.5: logarithm of returned power versus distance.

A.10.2 Distance with IQ-demodulator

The result is shown in figures A.8 and A.7. The standard deviation from the straight line was calculated to be 1.48 cm or 0.44°.

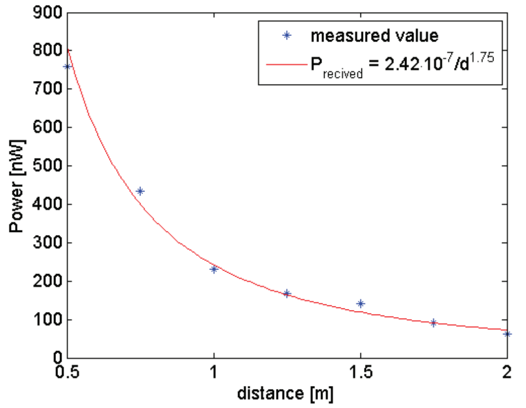

Figure A.6: Returned power versus distance.

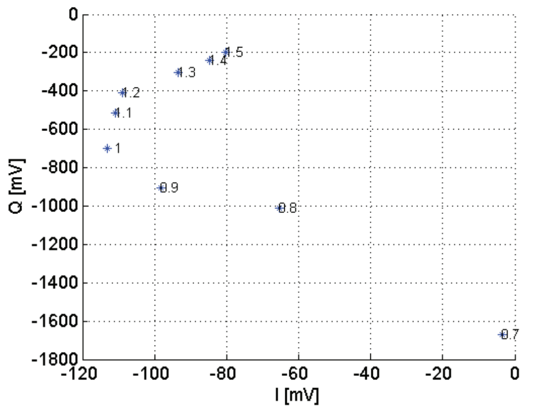

Figure A.7: The I- and Q-plane

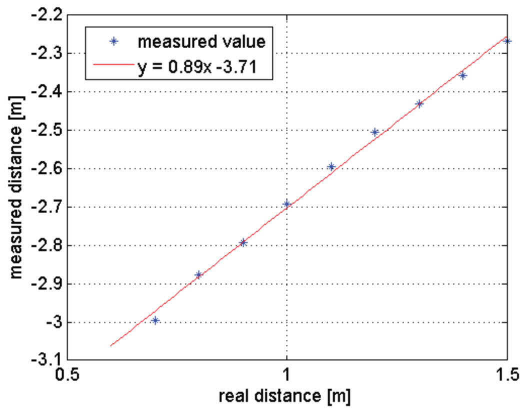

Figure A.8: Measured distance versus real distance.

A.11 Discussion

As mentioned above the results from the measurements with this first design were not satisfactory. The PCB had been modified to the extent that there was too much noise to do any meaningful measurements. The board however was instructive to design and study, but it did however manage to measure short distances and provided an indication that the concept worked.

A.11.1 Returned light distance relationship

Since the graph in figure A.6 shows a slope of -2, the received power is shown to be inversely proportional to the square of the distance, as was predicted by the theory. This measurement thus served as a first confirmation of this.

A.11.2 Distance with IQ-demodulator

The subsequent figures show that an the measured values of I and Q provide a crude approximation of the distance. The slope of the curve in figure A.8 does not have a slope of 1, which is expected. This error may be due to a number of reasons, but most likely it is due to inconsistent methods for measuring with the DSO.

A.11.3 Conclusion

The first design was successfully used to demonstrate that the received power decreased with the square of the distance. Furthermore, short distances were measured with some accuracy, but there was a scaling error which may depend on inconsistent measuring methods.

A.12 Summary

The first design had many problems such as bad signal integrity and many noise sources due to the heavy modification done to the PCB. The first amplifier stage worked fine for some photodiodes, but for others it oscillated and was not possible to stabilize. The ADA4817 with similar pin configuration was then tested and proved to be stable with all photodiodes, and was therefore employed in the second design.

The second stage amplifier was never made working, probably due to a footprint that was hard to solder by hand. As such, it was simply bypassed with a cord. Instead of this amplifier, another OPA847 in the inverting configuration was used, connected by a cord. This worked to some extent as more gain was obtained, but it was quite noisy to have a cord in the signal path.

The mixers were also bypassed by a cord, which due to a misunderstanding of the datasheet were never made operational.

In summary, the first design was nowhere near optimal, but it highlighted problems to be avoided in future designs, as well as to provide necessary training in PCB layout, soldering and practical mounting on the experiment setup.

Appendix B

Spice model for Laser diode

Script for the Laser diode model where different temperature could be modeled by changing to the corresponding curve from the datasheet. [54]

```
* LD = Laser diode cathode
* C = Common pin
* PD = Photodiode anode
.SUBCKT ADL65055TL LD C PD

* Laser diode power vs. current for 25 C
Eop op 0 TABLE {I(Vid)} (0,0) (18m,0.1m) (25m, 6m)

* uncomment for 40 C
*Eop op 0 TABLE {I(Vid)} (0,0) (21m,0.15m) (29m, 6m)

* uncomment for 50 C
*Eop op 0 TABLE {I(Vid)} (0,0) (0,0) (24m,0.2m) (32m, 6m)


Rdummy op 0 1k
* Monitor diode power vs. current
Gopd C PD TABLE {V(op)} (0,0) (30m,1.5m)
* Laser diode forward current and breakdown
Dld C I dlaser
Vid I LD
.model dlaser D IS=5E-37 N=1 RS=2 BV=2 IBV=10u
*EG=2.8 XTI=3
* Detector capacitance and breakdown
Dpd PD C pdetec
.model pdetec D CJO=5p BV=15 IBV=10u
.ends
```

Appendix C
Schematic

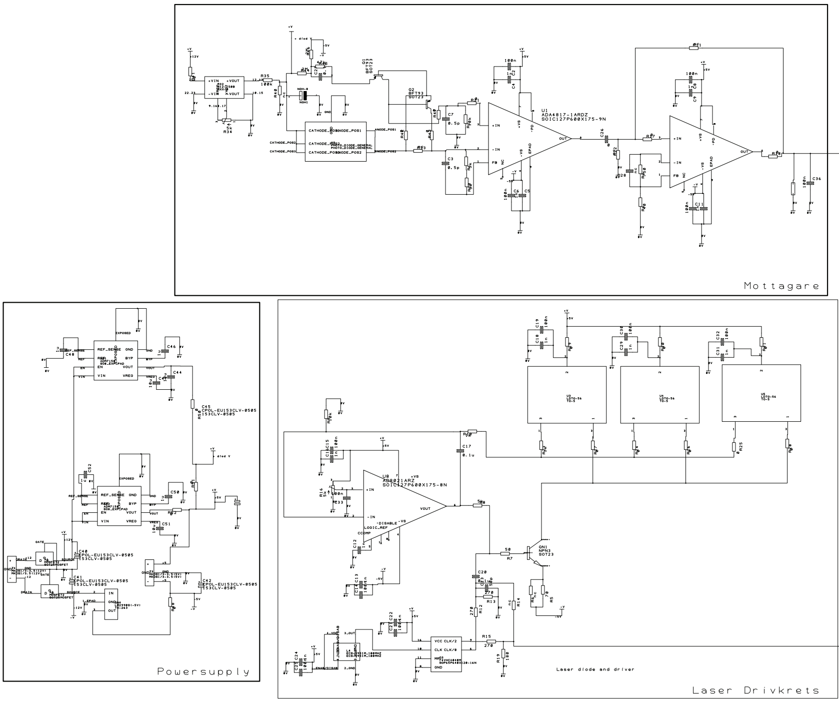

Figure C.1: Schematic for test the board.

Appendix D

MATLAB code for eye safe pulsed laser

D.1 Allowed emitted power versus pulse length and frequency

```
%plotting options
close all
FontSize = 13

%constants
texp = 0.25;
A = pi/4*0.7^2;
mpeSp = 5e-7;

%tested pulse length and frequencys
tpulsev = [5 20 200]*1e-9;
Prfv = logspace(4, 8, 1000);
P = zeros(length(tpulsev),length(Prfv));

%sweeping pulse length
j = 0;
tpulse = 0;
for tpulse = tpulsev
        j = j + 1;

    %sweeping pulse frequency
        i = 0;
        for Prf = Prfv
                i = i + 1;

        %checking eye safty
                n = Prf*texp;
                %rule 1
                P1 = mpeSp*A/tpulse;

                %rule 2
                mpeSpG = 1.8*0.25^0.75*1e-3/n;
```

```
                P2 = mpeSpG*A/tpulse;

                %rule 3
                mpeSpA = n^(-0.25)*mpeSp;
                P3 = mpeSpA*A/tpulse;

                P(j,i) = min(min(P1,P2),P3);
        end
end

%plot
figure (650)
loglog(Prfv,P*1e3)
xlabel('f [Hz]','FontSize',FontSize)
ylabel('P [mW]','FontSize',FontSize)
legend('5 ns', '20 ns', '200 ns')
grid
set(gca,'FontSize',FontSize)
```

D.2 Testing concept

```
%constants
texp = 0.25;
A = pi/4*0.7^2;
mpeSp = 5e-7;

%plotting font
FontSize = 13;

%sigma 50 m not normalised on power
aqnotnorm = 9.2234e-05 * 50.^2*2.5e-3;

%simulation interval
flv = 3*logspace(3, 6,100);
P = zeros(size(flv));
stdv = ones(size(flv))*1e6;

i = 0;
for fl = flv
        i = i + 1;

    %sweeping power
    for p = 1:-10^-4:0
        %sigmamax calc
        aq = aqnotnorm/p;
```

```
        %f_H calc
        fh = fl*2*pi/(aq*2);
        % pulse length
        tpulse = max(5/fh,100e-9);

        %checking eyesafty
        n = fl*texp;
        %rule 1
        P1 = mpeSp*A/tpulse;

        %rule 2
        mpeSpG = 1.8*0.25^0.75*1e-3/n;
        P2 = mpeSpG*A/tpulse;

        %rule 3
        mpeSpA = n^(-0.25)*mpeSp;
        P3 = mpeSpA*A/tpulse;

        %if comply find minimum std
        if(P1>p && P2>p && P3>p)
            std = aq*3e8/(fh*2*pi);
            if(std < stdv(i))
                P(i) = p;
                stdv(i) = std;
            end
        end

    end
end
stdv(stdv == 10^6)=0

%plotting results
figure(1)
%semilogx(flv, P*10^3)
semilogx(flv, stdv)
xlabel('f_{L} [Hz]','FontSize',FontSize)
ylabel('\sigma [m]','FontSize',FontSize)
grid
set(gca,'FontSize',FontSize)
```

Appendix E

Photodiode selection

Model	Type	Package	Sensitivity[1] [A/W]	Bandwidth	NEP [$fW/\sqrt{Hz}$]	Dark current [nA]	Capacitance [pF]	Reverse voltage[2]	Active area [mm2]	Price est. [dollar]
S10784 - Hamamatsu	PIN	Hole mounted	0.45	300 [MHz]	3.5	0.01	4.5	5	0.5[3]	12
PS0.25-5t - First sensor	PIN	smd, 1206	0.51	tr= 0.4ns	4	0.01	1.3	5	0.25	15
S1223 - Hamamatsu	PIN	Hole mounted TO-5	0.45	30 [MHz]	9.4	0.1	10	5	6.6	23
AD100-12 - First sensor	APD	smd, LCC6.1	0.43	tr= 0.12ns	2	0.05	0.5	75	0.008	117
S12023-10 - Hamamatsu	APD	Hole mounted TO-18	0.45	600[MHz]	-	0.2	6	135	0.8	121

Table E.1: Comparison of photodiodes. [1] Estimated from graph in respective datasheet.[2] Voltage at operation. [3] Plastic lens mounted which effectively gives active area of 7 mm^2.

LUND UNIVERSITY

http://www.eit.lth.se